Available online at www.sciencedirect.com

ScienceDirect

Journal of Materiomics 1 (2015) 153–169

www.ceramsoc.com/en/

www.journals.elsevier.com/journal-of-materiomics/

Review

High capacity group-IV elements (Si, Ge, Sn) based anodes for lithium-ion batteries

Huajun Tian [a], Fengxia Xin [a], Xiaoliang Wang [a,1], Wei He [a], Weiqiang Han [a,b,*]

[a] Ningbo Institute of Materials Technology and Engineering, Chinese Academy of Sciences, Ningbo 315201, China
[b] School of Physical Science and Technology, Shanghai Tech University, Shanghai 200031, China

Received 15 April 2015; revised 20 May 2015; accepted 9 June 2015
Available online 14 July 2015

Abstract

Tremendous efforts have been devoted to replace commercial graphite anode (372 mAh g^{-1}) by group IV elements (Si, Ge, Sn) based-materials with high capacities in lithium-ion batteries (LIBs). The use of these materials is hampered by the pulverization of these particles due to the high volumetric change during lithiation and delithiation cycles, which leads to particles pulverization and destabilization of solid electrolyte interphase (SEI) films. These problems result in fast capacity fading and low Coulombic efficiency. Nanostructured materials show significant improvements in rate capability and cyclability due to their high surface-to-volume ratio, reduced Li^+ diffusion length, and increased freedom associated with the volume change during cycling. However, the nanostructured active materials with high ratio of surface-to-volume increase the irreversible capacity due to the formation of more SEI films. Although the nanostructured materials active materials keep relatively stable during repeated cycles of lithiation/delithiation process, the SEI film continually breaks/reforms, lowing the Coulombic efficiency. Meanwhile, the high-cost, low Coulombic efficiency and low tapping density limit the commercialization of the nanostructured electrode materials. Therefore, it is urgent to find solutions which could take advantage of both long cycle life of nanomaterials within the group IV elements (Si, Ge, Sn) and high volumetric/gravimetric capacity of micro-materials in the group IV as well as elements (Si, Ge, Sn). This report presents an overview of the recently developed strategies for improving the group IV elements (Si, Ge, Sn)-based anodes performances in LIBs to provide a further insight understanding in designing novel anodes.

Keywords: High capacity; Group-IV elements; (silicon, germanium, tin) based anodes; Anodes; Lithium-ion batteries

1. Introduction

The group IV elements (silicon-Si, germanium-Ge, tin-Sn) have a much higher specific capacities (are 3579 mAh g^{-1},1600 mAh g^{-1}, 994 mAh g^{-1}, respectively) than that of commercial carbon-based anodes (372 mAh g^{-1}) [1–20]. They have been considered the most promising anode candidates for the next-generation LIBs. However, the use of bulk Si, Ge and Sn is hampered by the pulverization of the particles due to the high volumetric change of ~300% (are 297%, 270%, 257%, respectively) during lithiation and delithiation cycles, which leads to particle pulverization and destabilization of a solid electrolyte interphase (SEI) film. These problems result in fast capacity fading and low Coulombic efficiency. In the past 20 years, extensive efforts have been made to improve the electrochemical behavior of the group IV elements (Si, Ge, Sn)-based anodes. The most effective approaches mainly include: (1) reducing particle size to nanoscale for alleviating mechanical strain; (2) forming the hierarchical porous structure in order to provide a stable SEI layer and the inside pore providing adequate space for the group IV elements (Si, Ge, Sn) expansion; (3) dispersing nano-sized the group IV elements (Si, Ge, Sn) in a conductive matrix

* Corresponding author.
E-mail address: hanweiqiang@nimte.ac.cn (W. Han).
Peer review under responsibility of The Chinese Ceramic Society.
[1] Present address: Seeo Inc., 3906 Trust Way, Hayward, CA 94545.

http://dx.doi.org/10.1016/j.jmat.2015.06.002

(such as carbon-based materials) to accommodate volume change and maintain mechanical integrity of the composite electrode; (4) forming amorphous MO_x(M = Si, Ge, Sn) with small particle size. (5) narrowing down the voltage window and fixing the lithiation level. (6) using intermetallic alloys with a composite structure that contains an active or inactive host matrix.

In this work, we present an overview of recently developed strategies combined with our research group progress in the group IV elements (Si, Ge, Sn)-based anodes for improving their performances in LIBs. We hope to give a further understand of designing novel high-performance anodes.

2. High-capacity Si-based anodes

Among these (Si, Ge, Sn) anodes, Si has the highest specific capacity (3579 mAh g^{-1}) at a low charge–discharge potentials of <0.5 V (*vs.* Li/Li^+), corresponding to form the $Li_{15}Si_4$ phase, which delivers as 10 times higher theoretical specific capacity than that of conventional graphite anode [10,21–27]. The strategies to overcome the main problems, including low Coulombic efficiency, the unstable cycling life, low conductivity and tapping density, are summarized and discussed in this section.

Firstly, one successful method to alleviate mechanical strain induced by volume change of Si is to minimize the Si particle size to nano-scale, which has been proved to be an effective method. Nano-Si with a higher surface-to-volume ratio increases the irreversible capacity due to the formation of more SEI film. Although the nano-Si does not pulverize during repeated cycles of lithiation/delithiation process, the SEI film still continually breaks/reforms, lowing the Coulombic efficiency. Meanwhile, usually the nano-Si is very expensive of costly synthesis process and has low tapping density, which constrain the nano-Si commercialization.

In 1998, Wang et al. prepared nano-Si by ball-milling using micro-sized silicon mixed with graphite [28]. The nano-sized silicon particles could reversibly insert lithium, increase the capacity of the high lithium alloying capacity of silicon and retained the high reversibility of carbon. In 1999, Li et al. reported nanometer-scale Si powder as anode in LIBs prepared by laser-induced silane gas reaction method, which exhibited a high reversible capacity(1700 mAh g^{-1}) with better cycling performance than normal micro-sized Si [29]. The slurry weight ratio of Si, carbon black, and PVDF was 4:4:2. The electrochemistry testing indicated the nano-Si worked well even at a high current density. The authors suggested that enhanced performance was attributed to larger surface area, smaller diffusion length, and faster diffusion rate along extensive grain boundaries existing in nanoscale materials.

Secondly, nanostructuring of micro-sized electrode materials is considered as an effective solution to increase volumetric energy density and reduce the irreversible capacity. Hierarchical porous structure with carbon coating was designed in order to provide stable SEI layer and the inside pore provides adequate space for Si expansion.

Recently, Yi et al. successfully prepared porous micro-sized Si–C composite using SiO as the Si source, which demonstrated a high capacity of 1459 mAh g^{-1} and retained 97.8% of initial capacity after 200 cycles [30]. Micro-sized SiO was heated to form a Si/SiO_2 composite of interconnected Si nanoparticles embedded in a SiO_2 matrix due to the disproportionate of SiO. After etching, the SiO_2 was removed forming a large portion of the original pores. After that, the micro-sized porous Si was coated carbon by thermal decomposition of acetylene. Si and carbon were three-dimensionally interconnected in nano level, which could maintain internal electrical contact and sustain cycling stability.

Li et al. prepared a large (>20 μm) mesoporous silicon sponge by electrochemical etching of single crystal Si wafers. It delivered a capacity of ~1.5 mAh cm^{-2} with 92% capacity retention over 300 cycles [31]. The mesoporous Si sponge had a highly porous structure with thin crystalline Si walls surrounding large pores that were up to ~50 nm in diameter. Authors indicated that the suppression of pulverization and the low volume expansion of mesoporous Si sponge particles could summarized with three factors: (1) pores accommodate the Si volume expansion during lithiation; (2) ~10 nm Si walls are sufficiently thin that they reversibly expand/shrink during lithiation/de-lithiation without breaking; (3) solid surface oxide layer formed at the pore wall surface serves to confine and reinforce the nanostructures.

Kim et al. reported the 3D, porous Si particles, which consisted of bulk sizes greater than 20 μm. It was prepared by simple method using thermal annealing of SiO_2 particles and butyl capped Si gel at 900 °C under an Ar stream [32]. The capacity retention of this Si at a rate of 0.2C was 99% (~2800 mAh g^{-1}) after 100 cycles, while at a rate of 1C it was 90%. The capacities at a rate of 1, 2 and 3C were 2668, 2471, 2158 mAh g^{-1}, respectively. This work indicated that the superior rate capability was attributed to the interconnected 3D porous structure which provided fast lithium-ion mobility.

Tian et al. in our group also designed a hierarchical porous structure Si–C anode [33]. In this work, micro-sized (2–10 μm) Si/C composites consisting of 20 nm carbon coated secondary Si were synthesized from the abundant and low cost Al–Si alloy ingot by acid etching, ball-milling and carbonization procedures. The nano-porous Si/C composites provided capacity of 1182 mAh g^{-1} at a current density of 50 mA g^{-1}, 952 mAh g^{-1} at 200 mA g^{-1}, 815 mAh g^{-1} at 500 mA g^{-1}, and maintained 86.8% of initial capacity after 300 cycles. The superior rate capability and cycling stability of micro-sized nano-porous Si/C anodes are because it takes advantage of both long cycle life of nano-Si and high volumetric/gravimetric capacity of micro-Si. Al–Si ingot is quite cheap (~$2500/ton). The exceptional electrochemical performance and low cost scalable synthesis provide new diversion for high energy Li-ion batteries development. The synthesis of Si/C composite is schematically summarized in Fig. 1. Fig. 2a–b presented the electron microscope images of micro-sized porous Si after Al was etched out. The size was 2–10 μm and consisted of ~20 nm secondary Si and ~15 nm pores. XRD in Fig. 2f confirmed that Al was basically

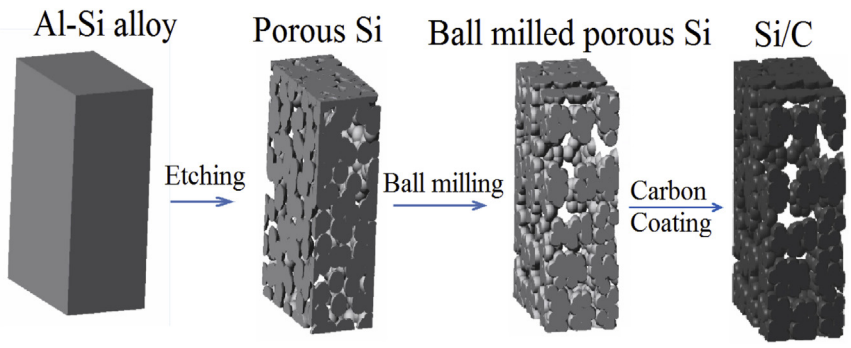

Fig. 1. Schematic illustration of the preparation process from Al–Si alloy to the Si/C composite (Reprinted with permission from Tian et al. [33]. Copyright 2015, Elsevier).

removed from the micro-sized eutectic Al–Si powders (JCPDS #27-1402), which was also confirmed by the energy dispersive X-ray spectra (EDS), Fig. 2c. The porous Si formed by etching Al–Si alloys normally showed poor cycling stability, due to the weak connection between Si dendrite in micro-sized porous Si [34]. To increase the connection between the Si particles in porous Si, porous Si was ball milled for 24 h. As shown in Fig. 2d–f, the ~2 μm porous Si (Fig. 2d and e) aggregated into 5 μm primary Si particles that consisting of 200 nm nano-Si cluster formed by ~20 nm Si particles. The nano-Si and nano-Si cluster were well connected each other, which would improve the cycling stability. Carbon coating on the micro-sized porous Si could greatly increase the rate performance and cycling stability. The SEM and TEM images of Si/C composite were illustrated in Fig. 2g–l. As shown in Fig. 2j–k, a layer of carbon with 15 nm thickness was uniformly coated on the nano-Si surface.

In this work, the low cost hierarchical structured porous Si/C anode retained 86.8% of initial capacity after 300 cycles at 500 mA g^{-1}, demonstrating one of the best performances for micro-sized low-cost Si (Table 1).

The doping approach has been proven useful for silicon anode materials, for example Al, Fe and B [33,45]. The mechanism of conductivity enhancement for Al and Fe doping in Si was investigated using the first-principle calculations. As shown in Fig. 3a, there are two sites for Al, Fe doping: silicon site (Si) and vacancy site (V). Al, Fe tended to co-doped silicon and form Al–Fe pairs (Al substituting the Si site and Fe occupying the vacancy site) [46]. Thus, Fe would mainly exhibit the Fe–Al co-doping pairs in the silicon sample. Fig. 3b and c showed the corresponding PDOS (atom-projected density of states) for spin-up and spin-down state of Al–Fe co-doped silicon, respectively. It could be seen that the spin-up state exhibited obvious impurity states near the Fermi level and the activation energy was about 0.2 eV, while the spin-down state affected less the edges of the Fermi level for doped silicon. The emerging impurity excitation was more favorable to increase the carrier concentration than intrinsic excitation, leading to higher electrical conductivity. On the other hand, the Al content was much higher than that of Fe, and the excessive Al atoms would form other point defects in the doped silicon sample. The PDOS of Al substituting the Si site and Al occupying the vacancy site were plotted in Fig. 3d and e. Al substituting the Si site and Al occupying the vacancy site would move the Fermi level toward the conduction bands and valence bands, respectively, which could increase the electron/hole concentration in systems, although no impurity states were introduced. Another benefit for partial Al-doping was that it could effectively prevent expanding of Si lattice (C (~10%), Al (~94%) and Si (~280% for amorphous Si), respectively, due to their different Li uptake capacities) [47]. Therefore, the low concentration Fe and Al impurities could increase the electrical conductivity, reduce the lattice expansion of silicon sample, and improve the performance of Si as anode materials in LIBs.

Third, one-dimensional(1D) Si nanomaterials possess efficient electron transport and allow lateral relaxation and reduced mechanical, leading to improvements in cycling stability, thus making them promising as anodes for high performance Li-ion batteries. Chan et al. synthesized silicon nanowires by vapor–liquid–solid process on stainless steel substrates using Au catalysts.[2] The Si NWs also displayed high capacities at higher currents. Even at the 1C rate, the capacities remained >2100 mAh g^{-1}. Silicon nanowire can accommodate large strain without pulverization, provide good electronic contact and conduction, and display short lithium insertion distances.

Ge et al. reported silicon nanowires synthesized by direct etching of boron-doped silicon wafers [48]. The reported porous silicon nanowires exhibited superior electrochemical performance and long cycle life. Even after 250 cycles, the capacity remained stable above 2000, 1600, and 1100 mAh g^{-1} at current rates of 2, 4, and 18 A/g, respectively. Porous silicon having a large pore size and high porosity could maintain its structure during long-term lithiation/delithiation process. Meanwhile, this work indicated that boron doping could increase electron conductivity in silicon, which would help to reach a high capacity at high current rates. On the other hand, the alginate as a binder, due to its high viscosity, could further improve the structural stability during long-term cycling.

Liu et al. reported a novel scaffold of hierarchical silicon nanowires-carbon textiles anodes fabricated via a CVD method [49]. The hierarchical structure Si NWs-carbon electrode exhibited high capacity (2950 mAh g^{-1} at 0.2C) and long cycle life (200 cycles). The excellent performance could

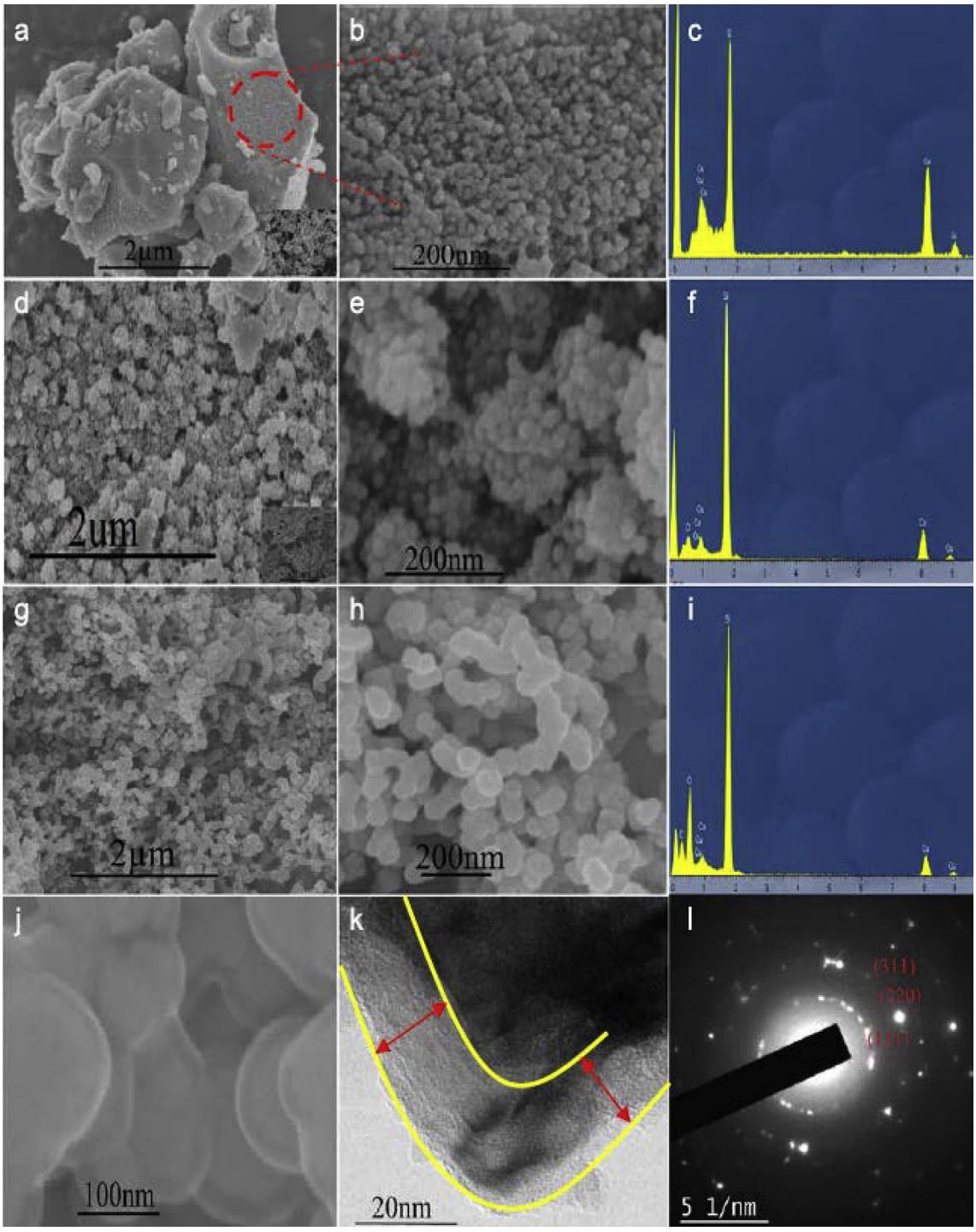

Fig. 2. Typical (a), (b) SEM images and (c) EDS of the prepared etched preliminary Si. (d), (e) SEM images and (f) EDS of ball milled etched Si. (g), (h), (j) SEM images and (i) EDS of Si/C composite. (k) HRTEM image of Si/C composite, (l) the selected area electron diffraction (SAED) patterns of the core in Si/C (Reprinted with permission from Tian et al. [33]. Copyright 2015, Elsevier).

be ascribed to: (1) 1D Si nanowires are beneficial to the insertion/extraction of Li^+; (2) the Si nanowires coated by carbon facilitates lithium-ion/electron transport; (3) the current silicon nanowires/carbon textiles matrix can obtain outstanding electronic conductivity.

Xue et al. prepared a new electrode composed of Si/C composite nanofibers using electrospinning method [50]. The mass loading of the active material was about 2 mg cm^{-2}. The cycling stability of the Si@C/CNF mat was improved and the capacity retention was increased to 92% in the first 15 cycles after by carbon coating. It was ascribed that the Si nanoparticles with a carbon layer enhanced the electric connection and bonding between Si particles and the fiber matrix.

Table 1
Comparison of electrochemical performance of micro-size Si based anodes in literature.

Si-based anodes	Si source	Particle size (μm)	Highest capacitances obtained (mAh g^{-1})	Capacity retention	Ref.
Si–C composite	Al–Si alloy ingot	2–10	952 mAh/g@0.2 A g^{-1}	86.8% capacity retention over 300 cycles	[33]
Silicon sponge	Si wafer	>20	790 mAh/g@0.1 A g^{-1}	~92.0% capacity retention over 300 cycles	[31]
Si–C composite	SiO	~20	1630 mAh/g@0.4 A g^{-1}	~97.8% capacity retention over 200 cycles	[30]
Porous c-Si	$SiCl_4$	>20	2800 mAh/g@0.4 A g^{-1}	~99.0% capacity retention over 100 cycles	[32]
Multi-dimensional Si–C	Si powder (30 μm, 99.9%)	5–8	~2400 mAh/g@~0.4 A g^{-1}	~95.0% capacity retention over 70 cycles	[35]
3D microporous Si–C	Si powder (10 μm, 99.9%)	~7	~2500 mAh/g@0.2 A g^{-1}	87.0% capacity retention over 50 cycles	[36]
C–Si nano-composite	SiH_4	15–35	~1950 mAh/g@~0.2 A g^{-1}	–	[1]
(Si–SiO–SiO_2)–C composite	SiO (325 mesh)	Micro size	~1280 mAh/g@0.2C	99.5% capacity retention over 200 cycles	[37]
Graphene/Si–C composite	SiO (2 μm)	Micro size	1100 mAh/g	After 100 cycles, ramains capacity of 3.2 mAh/cm^2	[38]
Prickle-like Si@C	Si powder	~5	1980 mAh/g@0.1 A g^{-1}	65.0% capacity retention over 100 cycles	[39]
Si–C composite	Triethoxysilane	Micro size	~1600 mAh/g@0.4 A g^{-1}	~90.0% capacity retention over 150 cycles	[40]
Si/C composites	Si powder (1–2 μm, 99.99%)	Micro size	1860 mAh/g@0.1 A g^{-1}	~68.9% capacity retention over 100 cycles	[41]
Graphene sheet-wrapped Si	Si powder	1–5	1525 mAh/g@0.2 A g^{-1}	After 30 cycles, ramains capacity of 1500 mAh g^{-1}	[42]
Si–C composite	Silicon powder (<78 μm)	Micro size	620 mAh/g@ 0.5C	After 50 cycles, ramains capacity of 525 mAh g^{-1}	[43]
Si@ self-healing polymer (SHP)	Silicon microparticles(3–8 μm)	Micro size	2617 mAh/g@0.4 A g^{-1}	80.0% capacity retention over 90 cycles	[44]

Xu et al. synthesized a novel flexible 3D Si/C fiber paper anode [51]. The flexible 3D Si/C fiber paper electrode demonstrated a very high overall capacity of ≈1600 mAh g^{-1} with capacity loss less than 0.079% per cycle for 600 cycles and excellent rate capability. The overall capacity still retained ≈500 mAh g^{-1} at a high current density of 8 A g^{-1}. The excellent performance was ascribed to the unique architecture of the flexible 3D Si/C fiber paper including the resilient and conductive carbon fiber network matrix, carbon-coated Si nanoparticle clusters, strong adhesion between carbon fibers and Si nanoparticle clusters, and uniform distribution of Si/C clusters in the carbon fiber frame.

Wang et al. prepared porous single-crystal silicon nanowires via an electroless HF/$AgNO_3$ etching process. The single-crystal silicon wafers [p-type, 0–100 Ωcm, (100)] were used as the silicon source [52]. In this work, the formed Ag nanoparticles were etched, and porous nanowires were formed (Fig. 4). Si nanowires with carbon black (NW + CB) as the conductive additive showed an initial capacity of 1066 mAh g^{-1}, as shown in Fig. 5a. The initial Coulombic efficiency was 49%. The capacity on the second cycle was 1256 mAh g^{-1}; after 20 cycles, it was 815 mAh g^{-1}, i.e., 76% of the initial value. Capacity retention was much better than that of solid nanowires. In the latter case, the capacity dropped by ~50% after 10 cycles. Furthermore, graphene nanosheets, massless charge carriers with high mobility were employed as effective 2D conductive additive to assure the high performance of Si nanowires. The NW + G (Si nanowire/graphene)

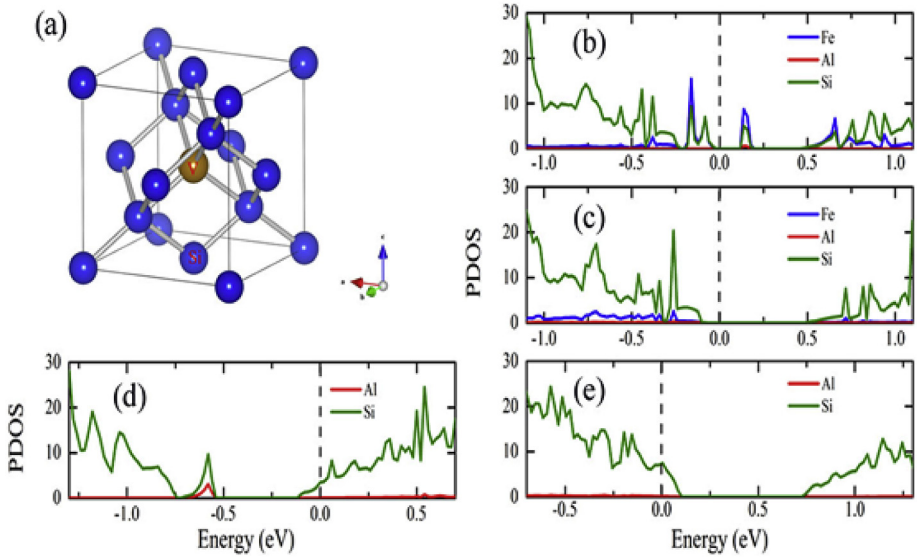

Fig. 3. The whole atomic is a cubic 3 × 3 × 3 supercell in first-principle calculations, (a) is part of the atomic model for doped silicon, and (b), (c), (d), (e) are the atom-projected density of states (PDOS) for Al, Fe codoping spin-up state, spin-down state, Al substituting the Si site (Si), and Al occupying the vacancy site (V), respectively (Reprinted with permission from Tian et al. [33]. Copyright 2015, Elsevier).

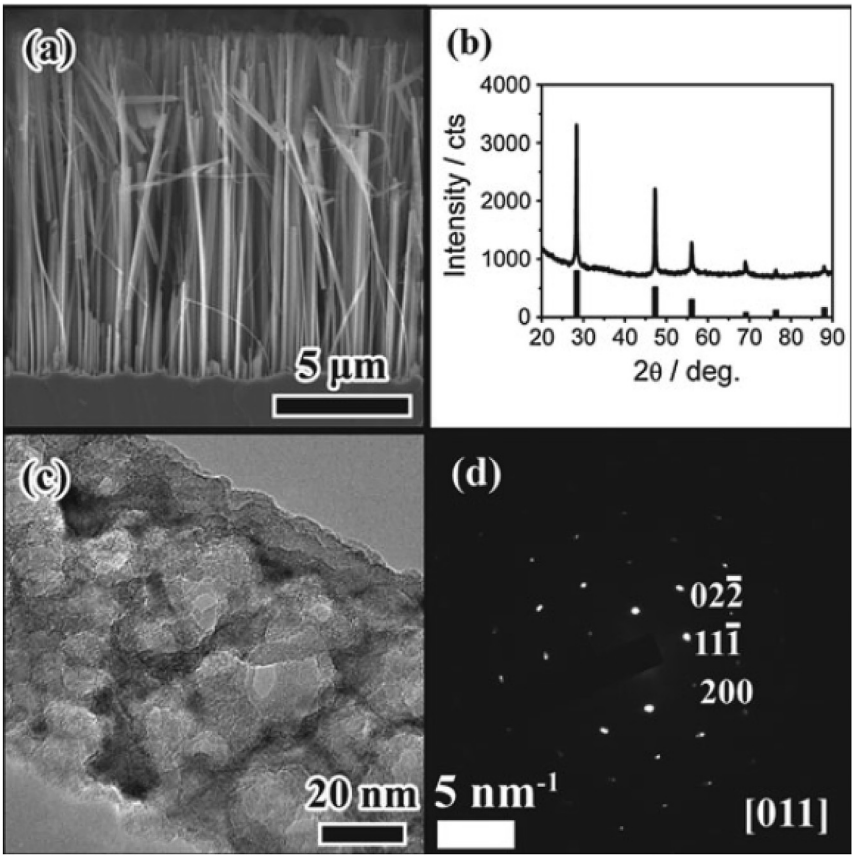

Fig. 4. Porous single-crystal Si nanowires. **a** SEM image of the wafer; **b** XRD patterns; **c** TEM image; and **d** SAED pattern along the [011] direction [15] (Reprinted with permission from Wang et al. [52]. Copyright 2010, The American Chemical Society).

anode had an initial capacity of 2,347 mAh g^{-1} (Fig. 5a). The Coulombic efficiency was 64% on the first cycle and quickly increased upon cycling, reaching close to 100%. Graphene could enhance the rate performance of Si nanowires. In this research, the electrochemical activity of Si nanowires with graphene was better than that of those with carbon black.

Overall, Si-based materials have been considered one of the most promising alternatives as anodes in LIBs. The main challenges for the practical implementation of Si-based anodes are the high volumetric change of ~300% during long-term lithiation and delithiation process and the unstable SEI films. However, breakthroughs have been achieved by the advanced nanotechnologies. Substantial process is needed to improve the first Coulombic efficiency, capacity retention and rate performance. It is believed that nanostructuring of micro-scale electrode materials is considered as an effective solution to increase volumetric energy density and reduce their reversible capacity. But it remains a challenge to develop a facile approach simultaneously solve the practical problems of Si-based anode materials including low first Coulombic efficiency, capacity retention, unsatisfied rate performance and fabrication costs.

3. High-capacity Ge-based anodes

Compared with Si, Ge has attracted less attention than Si because of its relatively higher cost. Nonetheless, Ge exhibits higher electronic conductivity (10^4 times) and lithium ion diffusivity (400 times) at room temperature than Si, which could exhibit higher rate performance as anode in LIBs [53–66]. However, similar to other Li alloy anodes, Ge-based anodes are hampered by the pulverization of the particles due to the high volumetric change of ~300%. To overcome those problems, many strategies have been utilized, mainly including: (1) using carbon as a buffer layer to mitigate the considerably large volume expansion; (2) decreasing the size of Ge-based particles to nanoscale; (3) adopting 3D porous structure in order to minimize and accommodate the volume changes of the Ge during lithiation/delithiation. (4) forming amorphous GeO_x with small size.

Electrochemical performances of reported Ge-based alloy anodes are summarized in Table 2. Xue et al. reported a facile method preparing Ge@C/RGO nanocomposite, which was used as an anode in LIBs [72]. After 50 cycles under a current density of 50 mA g^{-1}, the Ge@C/RGO nanocomposites still retained a reversible capacity of ~940 mAh g^{-1}. Even under the very high current density of 3600 mA g^{-1}, the Ge@C/RGO nanocomposites still exhibited a high specific capacity of 380 mAh g^{-1}. The authors indicated that this excellent performance could be ascribed to: (1) carbon shell acts as a buffer that plays a role to minimize volume changes; (2) RGO networks serve as the elastic and electronically conductive

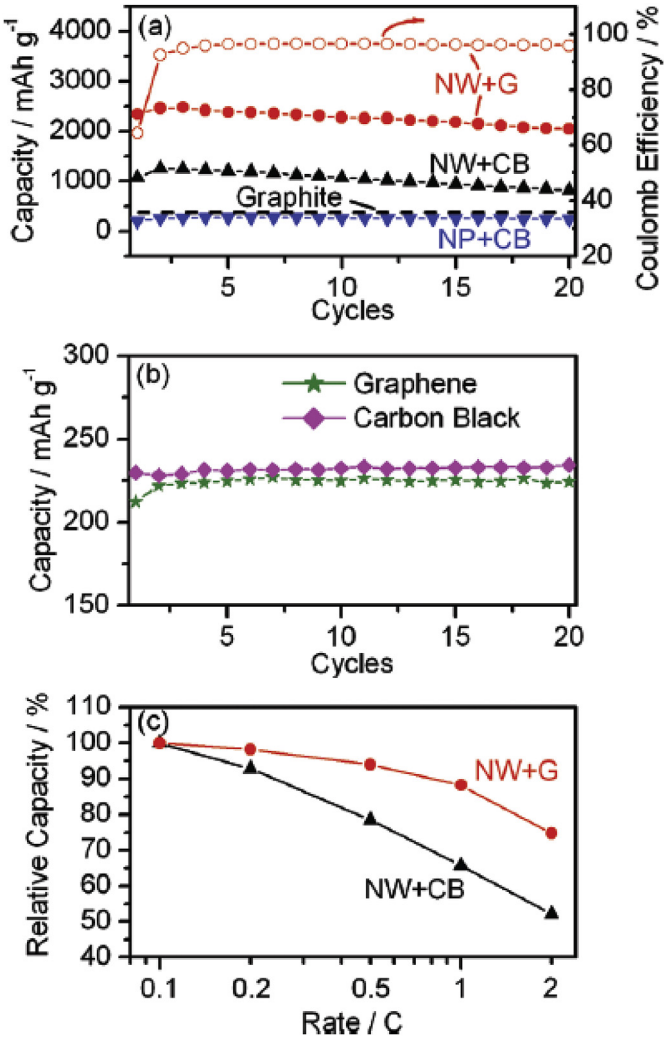

Fig. 5. (a) Charge capacities and Coulomb efficiency of cells for 20 cycles. NW: Si nanowires; G: graphene; CB: carbon black; NP: Si nanoparticles. We removed the contribution to capacity from graphene and carbon black (b). (c) Rate capacities from 0.1C to 2C, with the rate for discharge fixed to 0.1C (Reprinted with permission from Wang et al. [52]. Copyright 2010, The American Chemical Society).

substrate. It affords good dispersion of the NPs and guarantees a high electrical conductivity of the overall electrode.

Park et al. reported an amorphous GeO_2/C composite without carbon black as an electrode for Li-ion batteries [76]. The amorphous GeO_2/C electrode exhibited excellent electrochemical stability with a 95.3% charge capacity retention after 400 cycles. The authors also checked the practical applicability in full cell. The capacity of the full cell was reduced by only 7.6% after 50 cycles.

Cho et al. synthesized Ge nanoparticle from 0D Hollow to 3D Porous structure prepared by etching a thermally annealed physical mixture of SiO_2 and ethyl-capped Ge gels at 800 °C [77]. The first discharge capacities of the 0D and 3D could reach 1428 and 1380 mAh g^{-1}, respectively. The 3D porous Ge retained almost 99% of its capacity after 100 cycles at 1C rate.

Li et al. reported a novel approach via reduction and carbonization of germanium chelate synchronously to in situ forming uniform Ge with a size of about 30 nm dispersed uniformly in a carbon buffering layer [57]. This anode exhibited cycling capacity (ca. 895 mAh g^{-1}) over 2000 cycles at a high rate of 2C. The exceptional performance was attributed to the interconnected carbon buffering network and mesoporous structure.

Wang et al. reported 3D hierarchical porous structure amorphous GeO_x with very long cycle life (600 cycles) and high capacity (1250 mAh g^{-1}) [69]. The high-capacity GeO_x with its very long cycle life was ascribed to four beneficial characteristics: small primary particles, amorphous state, porous structure, and the incorporation of oxygen. Firstly, the primary small size could tolerate the change in volume, because the size of the particles was only ~3.7 nm (Fig. 6). Second, the electrical contact could be maintained because of the absolute volume change of each primary particle was small. Third, smallness may enhance electrochemical activity by shortening charge-transportation distances and offering more surfaces for charge transfer. In summary, the small primary particles were the basis for the hierarchical porous structure's stability and integrity upon high-capacity cycling. It also indicated that the amorphous state was another

Table 2
Comparison of electrochemical performance of Ge-based alloy anodes in literature.

Electrodes	Particle size	Initial Coulombic efficiency	Reversible capacity (mAh g^{-1})	Capacity retention	Ref.
GeO_2/Ge/C nanocomposite	30 μm	82%	1860 mAh g^{-1}@1C	90% over 50 cycles	[62]
Three-dimensional microporous Ge	700 nm	80.3%	1131 mAh g^{-1}@1C after 200 cycles	96.6% over 200 cycles	[67]
Ge/C nanowires	50–100 nm	82%	1200 mAh g^{-1}@0.2C after 50 cycles	84% over 50 cycles	[54]
Graphene/Ge nanowire	~46 nm	69%	1059 mAh g^{-1}@4C after 200 cycles	90% over 200 cycles	[68]
Amorphous hierarchical porous GeO_x	3.7 nm	70%	1268 mAh g^{-1}@C/2 after 600 cycles	96.7% over 600 cycles	[69]
Mesoporous Ge@C sphere	500 nm	87%	1099 mAh g^{-1}@0.1C after 100 cycles	–	[70]
Ge-carbon hybrid nanoparticles	200 nm	76%	895 mAh g^{-1}@2C after 2000 cycles	88% over 2000 cycles	[71]
Ge@C/RGO nanocomposite	10–15 nm	52%	940 mAh g^{-1}@50 mA g^{-1} after 50 cycles	–	[72]
Ge–RGO–CNT composites	20–30 nm	79.7%	863.8 mAh g^{-1}@100 mA g^{-1} after 100 cycles	–	[58]
Nano-GeO_2/mesoporous carbon composite	5–20 nm	–	452 mAh g^{-1}@1C after 380 cycles	93% over 380 cycles	[73]
GeO_2/RGO composite	30 nm	69%	1150 mAh g^{-1}@1C after 500 cycles	–	[74]
Ge@graphene/VAGN hybrids	42 nm	–	1014 mAh g^{-1}@260 mA g^{-1} after 90 cycles	97% over 90 cycles	[75]

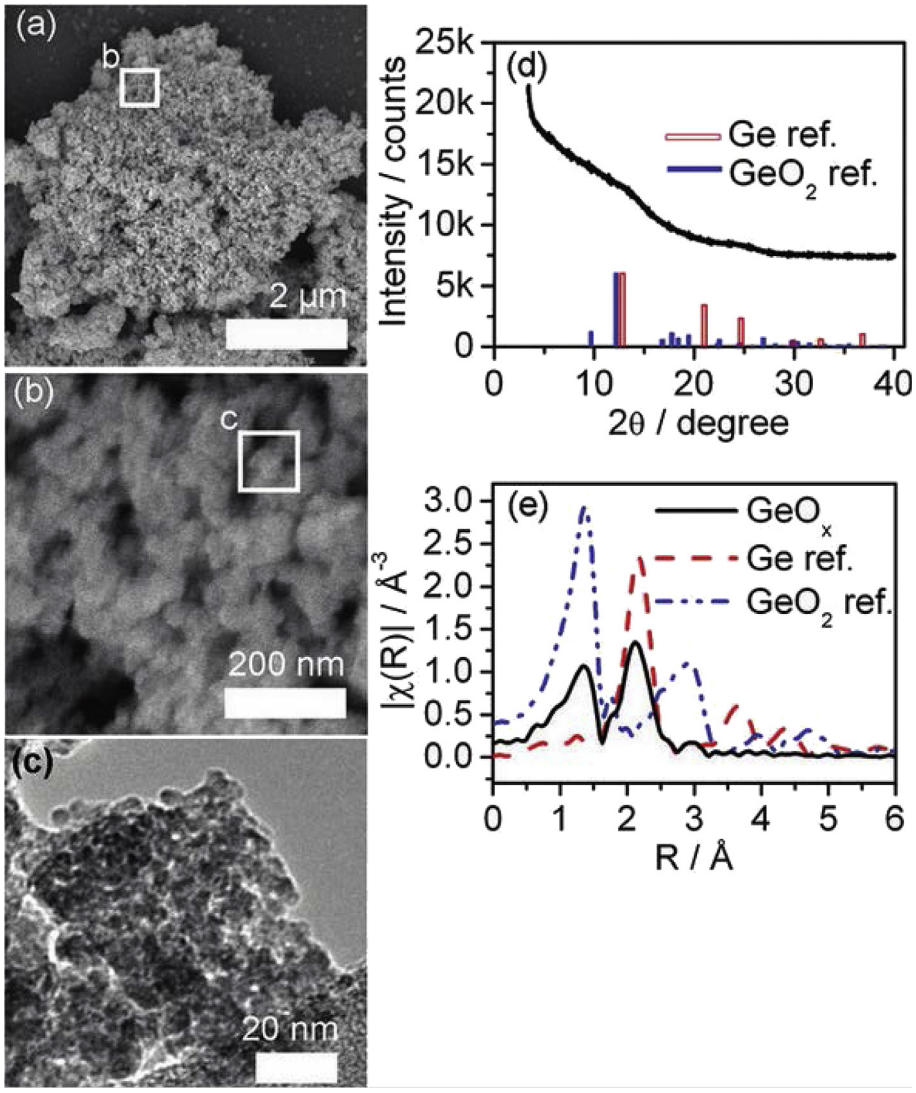

Fig. 6. Nano- and atom-structure of the initial GeO_x. a–c Hierarchical nanoporous structure, with **a** Low-magnification SEM image, **b** Enlarged SEM image corresponding to the area enclosed by a square in (a) and **c** TEM image corresponding to the area in the square in b d Synchrotron XRD profile ($\lambda = 0.72958$ Å). **e** Synchrotron EXAFS profile. Powder Diffraction File (PDF) peaks of Ge (#00-004-0545) and GeO_2 (#01-085-0473), and synchrotron EXAFSs of Ge and GeO_2 references, respectively, also are shown in (d) and (e) (Reprinted with permission from Wang et al. [69]. Copyright 2011, The American Chemical Society).

important factor. Ultrafine crystallites (<10 nm) still showed fading capacities that might be related to the harmful anisotropic expansion/extraction, and the stresses from phase transitions occurring in crystalline anode. Meanwhile, the hierarchical porous structure accommodated such alterations and preserved the intactness of the micron-sized GeO_x agglomerates, thus preventing changes in the microscopic charge-transport pathway and the particles' locations whilst maintaining the electrical contact. In Fig. 7, the GeO_x has a very stable capacity of ~1250 mAh g^{-1}, and retained its capacity very well for 600 full charge/discharge cycles.

The initial GeO_x was evaluated in full-cell configuration, a very challenging key step toward real-world applications. As shown in Fig. 8, it obtained an initial Coulombic efficiency of 99.5% with an open-circuit voltage (OCV) of 0.74 V. After that, $Li(NiCoMn)_{1/3}O_2$(NCM) was used as the active cathode in full cells. As shown in Fig. 8, a full cell discharged 164 mAh (g of NCM)$^{-1}$ at C/20 (based on $Li(NiCoMn)_{1/3}O_2$). The full cell exhibited stable charge/discharge cycling; and the average capacity loss over 200 cycles at C/2 was only 0.028% per cycle. Therefore, the initial GeO_x anode in a full cell had excellent reversibility and stability.

Compared with the silicon, Germanium has good lithium diffusivity and high electrical conductivity. However, the practical usage of Ge-based material as an anode is also hindered by dramatic volume changes caused by insertion/extraction of lithium ions, which results in crack and pulverization, and loss of electrode contact. Furtherly, because of its relatively higher cost, the performance of the Ge-based anodes still do not meet the commercial demands. The steadily improving performance of Ge-based anodes was attained through nanostructuring, carbon coating, porous and amorphous structuring et al. To gain commercial success, continued fundamental advances about the preparation, engineering and

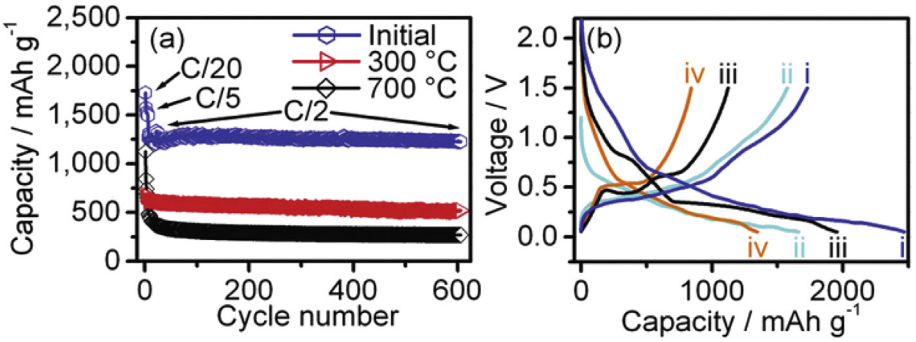

Fig. 7. Anode performance in half cells. **a** Delithiation capacities. **b** Charge-discharge curves. (i) The first cycle of the initial GeO_x (C/20). (ii) The second cycle of the initial GeO_x (C/5). (iii)The first cycle of the 700 °C sample (C/20). (iv) The second cycle of the 700 °C sample (C/5) (Reprinted with permission from Wang et al. [69]. Copyright 2011, The American Chemical Society).

fabrication need to execute for overcoming the technology barriers in high energy density LIBs.

4. High-capacity Sn-based anodes

Since Idota et al. showed that a tin-based amorphous oxide had a reversible Li-ion storage capacity >600 mAh g^{-1} [78], offering specific volume capacity >2200 mAh cm^{-3} corresponding to more than twice that of existing state-of-the art carbon materials, much attention has been focused on high capacity Sn-based anode materials [79–94]. In 2005, Sony's NP-FP71 lithium-ion batteries using the anode consisting of a Sn–Co based alloy (Sn:Co = ~1.1:1 mol, with possible titanium of ~5%) and graphite were commercialized. The particle sizes of the primary particles and the aggregated secondary particles for anode composite were ~5 nm and 1 μm, respectively [95]. The novel battery system, which alleviated the large volume change (257%) upon lithium insertion/extraction causing the pulverization of the particles and loosing electrical disconnection within the anode, was representative of the understanding tin alloys as anodes with high performance and exploring ideal second metal element.

Wang et al. successfully synthesized a series of M–Sn (M = Fe, Cu, Co, Ni) nanospheres [96] with size of 30–50 nm by a conversion chemistry [97–99], which could rigorously control both the shape and the size of these nanoparticles for comparing their different performances. The theoretical capacities are $CoSn_3$ (852 mAh g^{-1}) > $FeSn_2$ (804 mAh g^{-1}) > Ni_3Sn_4 (725 mAh g^{-1}) > Cu_6Sn_5 (605 mAh g^{-1}). However, the practical value of the alloy compounds could be listed in the following order: $FeSn_2$ > Cu_6Sn_5 ≈ $CoSn_3$ > Ni_3Sn_4. The higher capacity of $FeSn_2$ among these intermetallic nanospheres could be ascribed to open channels located within the $FeSn_2$ crystal lattice which promotes the penetration and alloying with Li in the Sn host.

During the synthesis of the Fe–Sn system, a reborn $FeSn_5$ phase, that is not in the Fe–Sn phase diagram representing a new binary structure type, was discovered as shown in Fig. 9 [100]. The crystal structure including lattice parameters, thermal factors, atomic coordinates, and occupancies was solved using the charge-flipping method. Differing from room-temperature FeSn and $FeSn_2$ phases, and high-temperature Fe_5Sn_3 and Fe_3Sn_2 phase, new $FeSn_5$ phase belongs to tetragonal in the P4/mcc space group. Fe vacancies always exist in the pure intermetallic $FeSn_5$, implying strongly that the stable $FeSn_5$ structure could maintain in the condition of existing large numbers of Fe vacancies. Structurally, the

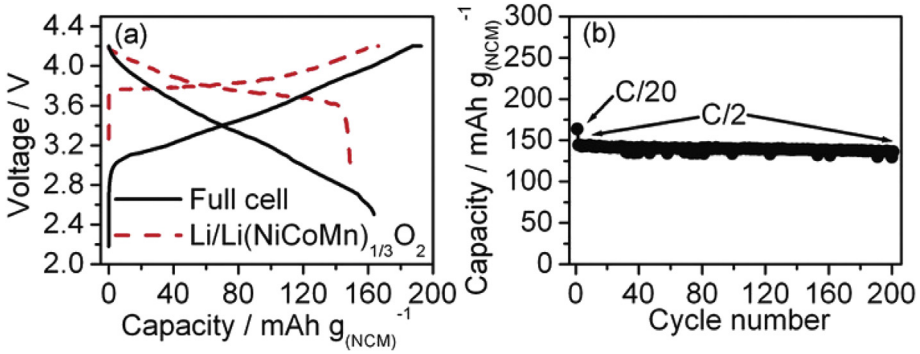

Fig. 8. Cell performance of the initial GeO_x anode. **a** Initial profiles of the Li-compensated GeO_x/NCM full cell in comparison with those of the Li metal/NCM half-cell. **b** Reversible battery discharge capacity of NCM in the full cell (Reprinted with permission from Wang et al. [69]. Copyright 2011, The American Chemical Society).

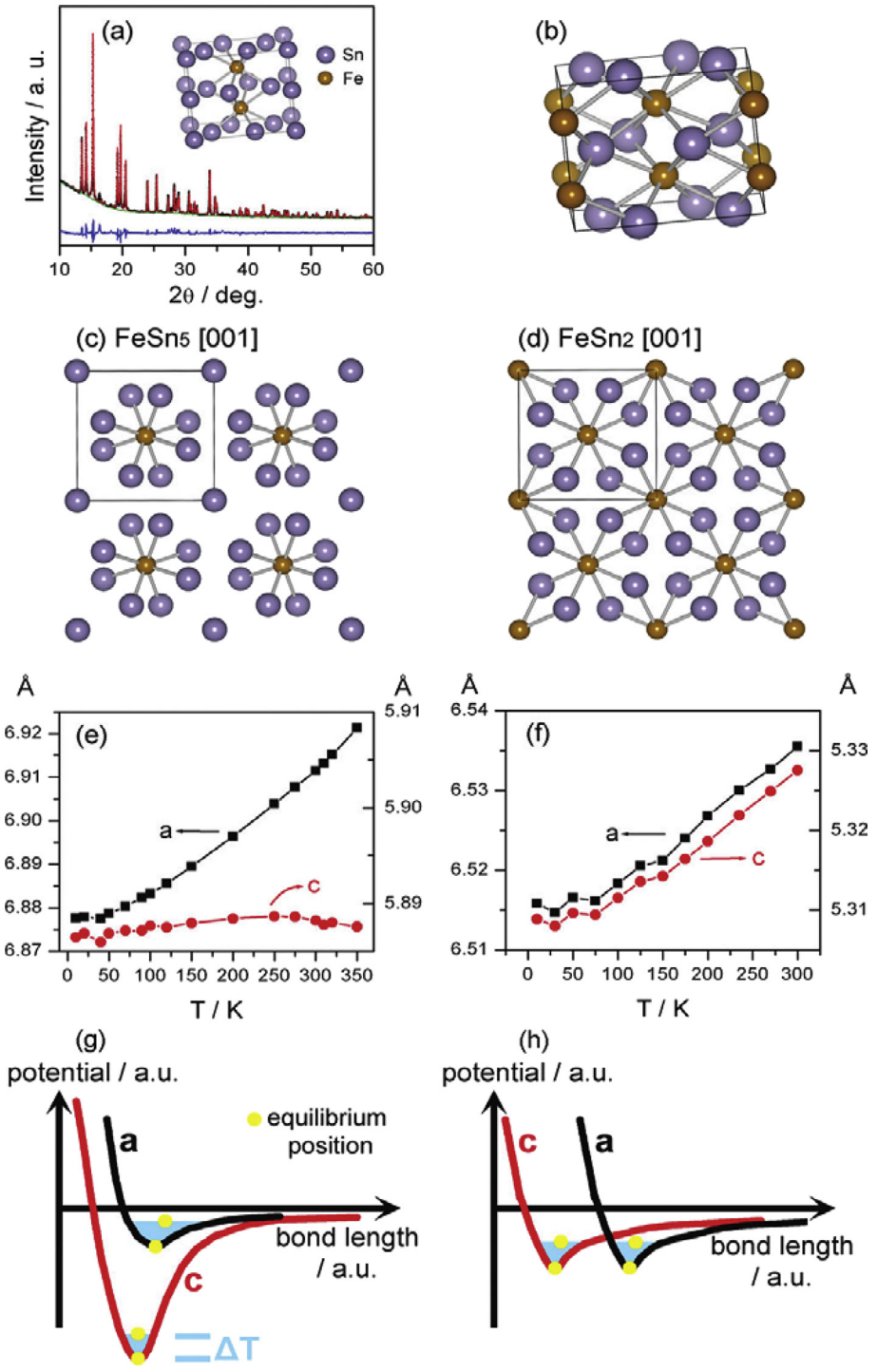

Fig. 9. (a) Synchrotron XRD pattern and Rietveld refinement of $Fe_{0.74}Sn_5$. Black dots, observed profile; red line, calculated profile; blue line, difference profile; and olive line, background, with the inset illustrating the crystal structure. (b) The crystal structure of $FeSn_2$, in which the color designation is the same as (a). (c) $Fe_{0.74}Sn_5$ and (d) $FeSn_2$ crystal structures from [001] view direction. (e and f) The variation of lattice constants with temperature, (e) $Fe_{0.74}Sn_5$ and (f) $FeSn_2$. (g and h) The illustration of bond energy diagrams showing the influence of temperature on the thermodynamic equilibrium lattice parameters a and c, (e) $Fe_{0.74}Sn_5$ and (f) $FeSn_2$ (Reprinted with permission from Wang et al. [100]. Copyright 2011, The American Chemical Society).

antiprisms form only weakly interconnected a one-dimensional (1D) network along the c-axis in $FeSn_5$, leading to strong quasi-1D characteristics, drastically different from the 3D network of $FeSn_2$. The $Fe_{0.74}Sn_5$ nanospheres (~45 nm) possesses the highest theoretical capacity of 929 mAh g^{-1} among the reported M (electrochemically inactive metal)-Sn intermetallic anodes by then.

During the preparation of the Co–Sn system, an almost identical crystal structure as $FeSn_5$ binary intermetallic phase was achieved by $CoSn_5$ due to similarity between Fe and Co

[101]. The $Co_{0.83}Sn_5$ (Co-deficient $CoSn_5$) anode demonstrated one of best-in-class theoretical capacity of 917 mAh g^{-1} among the existing Sn–M alloys. The cell exhibited very good capacity retention (ca. 450 mAh g^{-1}) over 100 cycles at a rate of 0.05C. The increase in cycle capacity early in the cycling of the $Co_{0.83}Sn_5$ alloy could be ascribed to (i) an activation process of anode (especially for high capacity electrodes with large volume expansion/shrinkage) in initial few lithiation/delithiation cycles (ii) the formation and stabilization of the SEI (iii) the improvement of Li uptake/removal kinetics (iv) an electrode structural readjustment upon lithium insertion/extraction (v) the creation of new electrical contacts between nanospheres/carbon black (vi) the reaction of a thin oxide shell with lithium.

Fe and Co atoms could co-exist in the MSn_5 structure, forming $Fe_{0.5}Co_{0.5}Sn_5$ ternary structure, which had the highest theoretical capacity of 931 mAh g^{-1} to date among the reported Sn-based ternary intermetallic anodes [102]. Monodisperse 30–50 nm MSn_5 (M = Fe, Co and FeCo) nanospheres were obtained by using Sn nanospheres as templates by conversion chemistry strategy. The formation mechanism of $FeSn_5$, $Fe_{0.5}Co_{0.5}Sn_5$, $CoSn_5$ nanospheres was schematically summarized in Fig. 10a. In this work, 30–50 nm tin nanospheres were synthesized in a three necked flash by adding of $SnCl_2$ into a hot tetraethylene glycol (TEG) solution containing surface stabilizers (PVP and PEtOx) at 170 °C, followed by reduction with sodium borohydride ($NaBH_4$). With the increasing of the temperature of Sn mixture to 205 °C, 200 °C, 195 °C, followed by the adding of $FeCl_3$/TEG, $FeCl_3$ + $CoCl_2$/TEG, $CoCl_2$/TEG solution, precipitates metal Sn nanocrystals had been converted to intermetallic compounds $FeSn_5$, $Fe_{0.5}Co_{0.5}Sn_5$, $CoSn_5$ NCs, typically via diffusion-based processes where Fe/Co diffused into Sn. The similar particle distribution of these three compounds was demonstrated using electron microscope images in Fig. 10b, e, h. HRTEM images revealed that all nanospheres had core–shell structure consisting of a ~30 nm single-crystalline intermetallic core and a ~4 nm amorphous oxide shell (Fig. 10c, f, i). The STEM EDS elemental mapping images clearly demonstrated homogeneous distribution of transition metals (Fe or Co) and Sn in the nanospheres with the ratios 7:1, 7:1, and 6:1 for the Sn/Fe, Sn/Fe + Co respectively as evidenced by TEM-EDS.

The reversible reactions mechanism during the first lithiation/de-lithiation cycle for these compounds could be described as:

$$x\mathrm{Li} + \mathrm{M}_y\mathrm{Sn}_5 \leftrightarrow \mathrm{Li}_x\mathrm{M}_y\mathrm{Sn}_5 (\mathrm{M} = \mathrm{Fe},\ \mathrm{Co\ or\ FeCo}, 0.7 - 0.3\ \mathrm{V}); \quad (1)$$

$$z\mathrm{Li} + \mathrm{Li}_x\mathrm{M}_y\mathrm{Sn}_5 \leftrightarrow \mathrm{Li}_{x+z}\mathrm{Sn}_5 + y\mathrm{M} (x + z \le 22, 0.3 - 0.01\ \mathrm{V}); \quad (2)$$

At the first discharge process (Fig. 11), the formation of Li–Sn alloy could be responsible for the reversible capacity up to the theoretical limit of $Li_{4.4}Sn$. Further charge to 1.5 V, the reformation of MSn_5 phase was attributed to high reversibility, differing from known Fe–Sn or Co–Sn phases. $FeSn_5$ anode exhibited a high specific capacity of 750 mAh g^{-1} along with dramatic derogation after 15 cycles due to gradually separation of Sn from Fe aggregated into large particle in $FeSn_5$ phase. After 100 cycles under a current density of 0.05C, the $CoSn_5$ intermetallic nanospheres still retained a reversible capacity of ~460 mAh g^{-1} which was attributed to alloying of Sn and Co although the ratio of Sn to Co decreases from 6:1 to 4:1. $Fe_{0.5}Co_{0.5}Sn_5$ phase can take advantages of high capacity and cycling life, providing 736 mAh g^{-1} and maintaining 92.7% of initial capacity after 100 cycles with an average capacity loss of only 0.07% per cycle. The performance of reported Sn-based alloy anodes are summarized in Table 3. These works provide insight towards exploring and designing new Sn-based alloy anode materials for Li-ion batteries.

By introducing carbon matrices with high electrical conductivity, good mechanical stability and the ability to store lithium for Sn electrode is one of successful methods to effectively accommodate the strain caused by the volume expansion/shrinking and provide good electronic conductivity for overall electrode. Graphite, carbon nanotubes (CNT), graphene, ordered mesoporous carbon and amorphous carbon are usually exploited as conductive network and an inert for Sn-based materials, offering many different Sn/C composite anode including Sn@carbon nanoparticles in bamboo-like hollow carbon nanofibers [115], Sn@C@CNT nanostructures [116], graphene-confined Sn nanosheets [117], 3D hollow Sn@carbon-graphene hybrid material [118] et al.

In 2013, Wang's group reported nano-Sn/C composite with uniformly dispersed 10 nm nano-Sn within a spherical carbon matrix using facile and scalable aerosol spray pyrolysis technique [119]. The nano-Sn/C composite sphere exhibited excellent electrochemical stability with charge capacity of 710 mAh g^{-1} after 130 cycles at 0.25C. Even at a high rate of 20C, discharge capacity could maintain high rate performance (~600 mAh g^{-1}). The exceptional performance of nano-Sn/C anodes was attributed to the carbon matrix to accommodate the stress, prevented Sn nanoparticle agglomeration and provided continuous path for charge transfer. In 2013, Zhu et al. reported ultrasmall Sn nanoparticles (~5 nm) embedded in nitrogen-doped porous carbon network by carbonizing of Sn at 650 °C under Ar atmosphere [120]. The initial discharge capacity of Sn/C anode could reach 1014 mAh/g with 71.2% capacity retention over 200 cycles at the current density of 0.2 A/g. At higher current density of 5 A/g, the reversible capacity could still retain ~480 mAh/g. The remarkable electrochemical performance can be summarized as follows: ultrasmall Sn nanoparticles, homogenous distribution, and porous carbon network structure. 2014, Qin et al. fabricated 5–30 nm Sn nanoparticles anchoring 3D porous graphene networks encapsulated in 1 nm graphene shells by using NaCl particles as a template with a three-dimensional (3D) self-assembly and metal precursors as a catalyst [121]. The 3D hybrid anode showed excellent rate performance that 1022 mAh g^{-1} at 0.2C, 865 mAh g^{-1} at 0.5C, 780 mAh g^{-1} at 1C, 652 mAh g^{-1} at 2C, 459 mAh g^{-1} at 5C, and

270 mAh g^{-1}at 10C could be obtained. At high rate (2 A/g), the anode had extremely long cycling stability that high capacity could reach 682 mAh g^{-1} and maintain 96.3% charge capacity retention after 1000 cycles.

Xin et al. synthesized $Fe_{0.74}Sn_5$@RGO nanocomposite which could achieve capacity retention 3 times than that of the nanospheres alone after 100 charge/discharge cycles by a one-pot wet chemistry synthesis [122]. The excellent electrochemical performance of $Fe_{0.74}Sn_5$@RGO nanocomposite could be related to the following characteristics: (1) the flexible and conductive RGO sheets offers mechanical support to accommodate the stress from large volume change during charge/discharge process; (2) RGO sheets prevent $Fe_{0.74}Sn_5$ nanoparticle agglomeration can relieve irreversible aggregation and/or stacking of individual RGO nanosheets. (3) RGO sheets provide good electrical conductivity (4) large voids between the nanoparticles and RGO sheets promote easy penetration of the electrolyte. Similar with Si and Ge anode, the small size of primary particles and porous structure can effectively alleviate mechanical strain resulted from volume fluctuation [123,124].

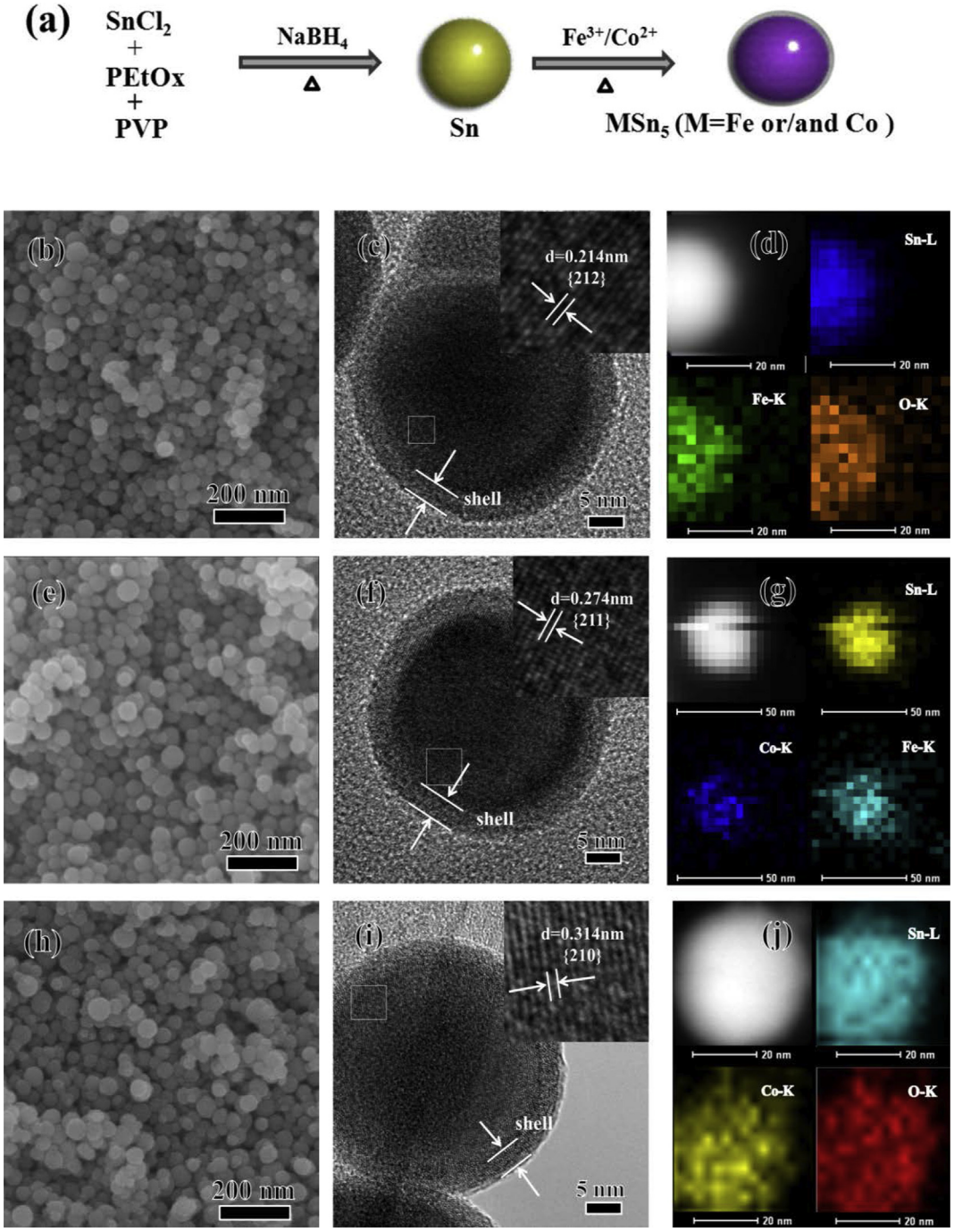

Fig. 10. (a) Synthesis process for $FeSn_5$, $Fe_{0.5}Co_{0.5}Sn_5$ and $CoSn_5$ nanospheres; (b, e, h) SEM; (c, f, i) HRTEM; and (d, g, j) STEM-EDS elemental mappings images of $FeSn_5$, $Fe_{0.5}Co_{0.5}Sn_5$ and $CoSn_5$ nanospheres (Reprinted with permission from Xin et al. [102]. Copyright 2015, Royal Society of Chemistry).

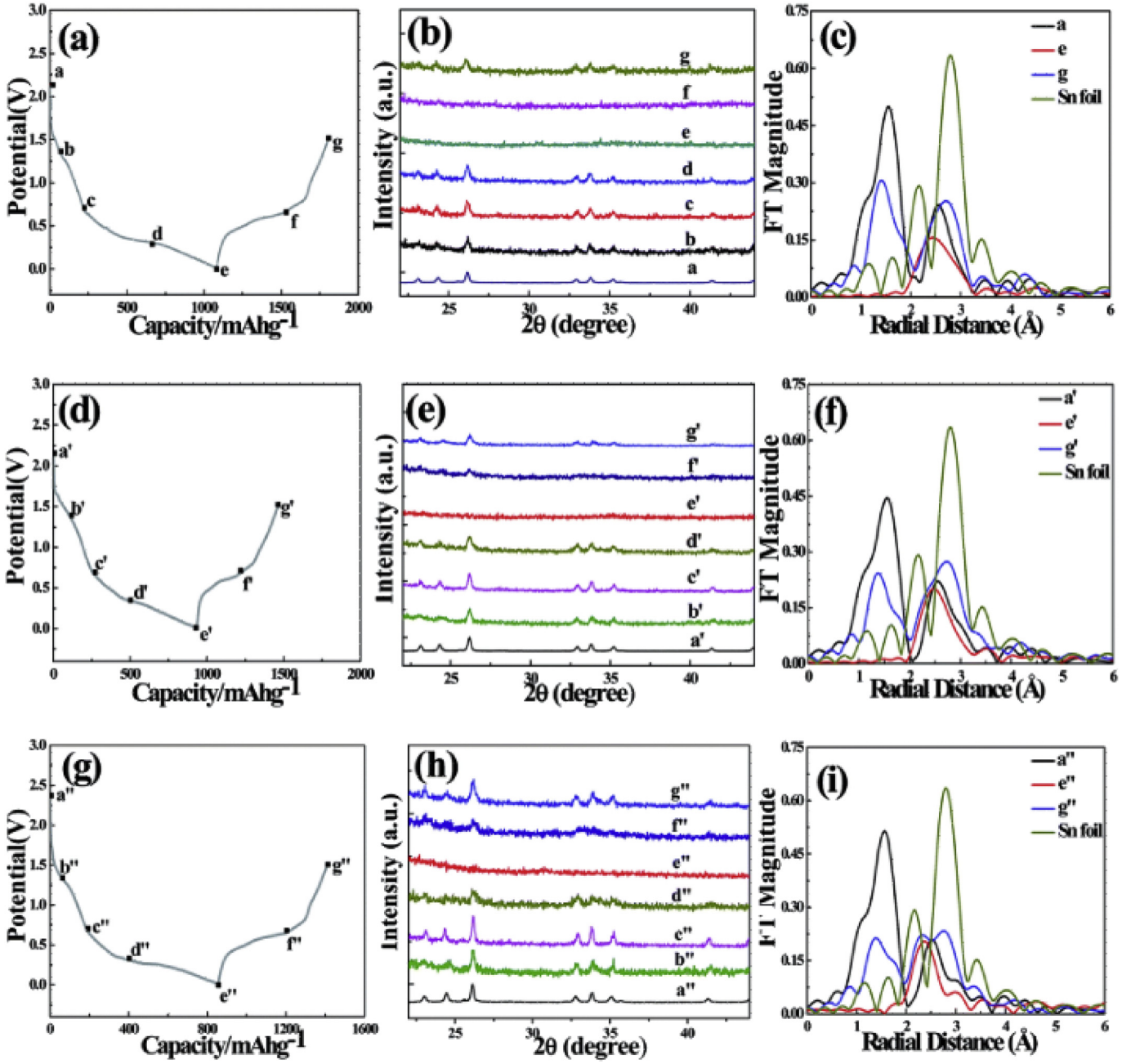

Fig. 11. (a, d, g) Charge and discharge curves of the $FeSn_5$, $Fe_{0.5}Co_{0.5}Sn_5$ and $CoSn_5$ nanospheres electrode for the first cycle at a current density of 0.05C; (b, e, h) Synchrotron ex situ XRD patterns of at different potentials during discharge and charge processes of $FeSn_5$, $Fe_{0.5}Co_{0.5}Sn_5$ and $CoSn_5$ nanospheres electrode and (c, f, i) the set of FTs of the Sn K-edge XAFS spectra taken during the first cycle (Reprinted with permission from Xin et al. [102]. Copyright 2015, Royal Society of Chemistry).

We summarized the general method to address the problems of Sn-based anodes, including: (1)using Sn−M or Sn−M−C alloys(M = Fe, Cu, Co, Ni); (2)reducing the particle size of Sn to nanoscale; (3)intergrating nano-Sn with a conductive matrix such as carbon. Especially, among M−Sn intermetallics, sustained effort has been devoted to develop high capacity Fe−Sn, Co−Sn, Fe−Co−Sn systems in the academic and industry. It is quite promising that continual development of these and other strategies will promote the practical applications of Sn-based anodes material in LIBs.

5. Conclusions

The group IV elements (Si, Ge, Sn)−based anodes have been considered very promising anodes in the next-generation LIBs due to their high capacities. In the past 20 years, great efforts have been made in exploring group IV elements (Si, Ge, Sn) based-anodes with high energy/power density, good cycling stability, environmental friendliness, and low cost for practical applications. However, the use of bulk Si, Ge and Sn is always hampered by the pulverization of the particles due to

Table 3
Comparison of electrochemical performance of Sn-based alloy anodes in literature.

Sn-based alloy anodes	Method	Particle size (nm)	Highest capacitances obtained (mAh g^{-1})	Capacity retention	Ref.
M–Sn (M = Fe, Cu, Co, Ni)	Conversion chemistry	~40	~510, 350, 280, 250 mAh/g@0.05C	~94.1, 71.4, 94.6, 76% capacity retention ≥100 cycles	[96]
$FeSn_5$	Conversion chemistry	30–50	768 mAh/g@0.05C	78.9% capacity retention ≥20 cycles	[100]
$CoSn_5$	Conversion chemistry	30–50	548 mAh/g@0.05C	~81.8% capacity retention over ≥100 cycles	[101]
$Fe_{0.5}Co_{0.5}Sn_5$	Conversion chemistry	30–50	736 mAh/g@0.05C	~71.0% capacity retention ≥100 cycles	[102]
Cu_6Sn_5	Chemical reduction	~40	815 mAh/g@0.1 mA cm^{-2}	~33.0% capacity retention ≥100 cycles	[103]
Cu_6Sn_5–Sn	Electrodeposition	Micro size	1020 mAh/g@0.08 mA cm^{-2}	~34.3% capacity retention ≥55 cycles	[104]
Cu_6Sn_5	Electron beam deposition	~100	720 mAh/g@50 mA g^{-1}	~76.4.0% capacity retention ≥15 cycles	[105]
Sn_2Fe:$SnFe_3C$	Ball-milling	~10–20	~650 mAh/g@37 mA g^{-1}	48.3% capacity retention ≥40 cycles	[106]
$FeSn_2$	Chemical reduction	30–70	~635 mAh/g@80 mA g^{-1}	78.7% capacity retention ≥20 cycles	[107]
$Fe_{0.5}Co_{0.5}Sn_2$	Reduction	~20	~750 mAh/g@80 mA g^{-1}	73.3% capacity retention ≥30 cycles	[108]
$[Sn_{0.55}Co_{0.45}]_{1-y}C_y$	Sputtering	–	700 mAh/g@C/12	–	[109]
$Sn_{31}Co_{28}C_{41}$	Ball milling	Nano Size	~500 mAh/g@0.25C	100.0% capacity retention ≥100 cycles	[110]
Sn–Co–C	Mechano-chemical	~50	478 mAh/g@100 mA g^{-1}	~91% capacity retention ≥100 cycles	[111]
Ni_3Sn_2	Electron beam deposition	10	800 mAh/cm^3@30 uA cm^{-2}	~100% capacity retention ≥500 cycles	[112]
Sn–Ni	Electrodeposition	Nano Size	~800 mAh/g@250 mA g^{-1}	~82.5% capacity retention≥70 cycles	[113]
Ni_3Sn_2	Solvothermal route	2–5	~771 mAh/g@0.2C	~90.3% capacity retention ≥400 cycles	[114]

the high volumetric change during the lithium insertion/extraction process, which causes electrode agglomeration, pulverization, and thus fast capacity fading. In this article, we not only review the main problems of group IV elements (Si, Ge, Sn)-based materials as anodes in LIBs, but also introduce the main solutions, especially using our group works as examples. The main solutions are summarized as: (1) reducing particle size to nanoscale for alleviating mechanical strain; (2) forming the hierarchical porous structure in order to provide stable SEI layer and the inside pore to provide adequate space for (Si, Ge, Sn) expansion; (3) using carbon as a buffer layer to accommodate volume change and maintain the mechanical integrity of the composite electrode; (4) narrowing the voltage window and fixing the lithiation level. (5) forming amorphous MO_x(M = Si, Ge, Sn) with small size. (6) using intermetallic alloy with a composite structure that contains an active or inactive host matrix.

Acknowledgments

This work was financially supported by the National Natural Science Foundation of China (Grant No. 51371186), the "Strategic Priority Research Program" of the Chinese Project Academy of Science (Grant No. XDA09010201), Zhejiang Province Key Science and Technology Innovation Team (Grant No. 2013TD16), Ningbo 3315 International Team of Advanced Energy Storage Materials, and Ningbo Natural Science Foundation (Grant No. 2014A610046).

References

[1] Magasinski A, Dixon P, Hertzberg B, Kvit A, Ayala J, Yushin G. High-performance lithium-ion anodes using a hierarchical bottom-up approach. Nat Mater 2010;9:353–8.
[2] Chan CK, Peng HL, Liu G, McIlwrath K, Zhang XF, Huggins RA, et al. High-performance lithium battery anodes using silicon nanowires. Nat Nanotechnol 2008;3:31–5.
[3] Armand M, Tarascon JM. Building better batteries. Nature 2008;451:652–7.
[4] Goriparti S, Miele E, De Angelis F, Di Fabrizio E, Zaccaria RP, Capiglia C. Review on recent progress of nanostructured anode materials for Li-ion batteries. J Power Sources 2014;257:421–43.
[5] Terranova ML, Orlanducci S, Tamburri E, Guglielmotti V, Rossi M. Si/C hybrid nanostructures for Li-ion anodes: an overview. J Power Sources 2014;246:167–77.
[6] Wang XH, Susantyoko RA, Fan Y, Sun LM, Xiao QZ, Zhang Q. Vertically aligned CNT-supported thick Ge films as high-performance 3D anodes for lithium ion batteries. Small 2014;10:2826–9.
[7] Sourice J, Quinsac A, Leconte Y, Sublemontier O, Porcher W, Haon C, et al. One-step synthesis of Si@C nanoparticles by laser pyrolysis: high-capacity anode material for lithium-ion batteries. ACS Appl Mater Inter 2015;7:6637–44.
[8] Ryu J, Choi S, Bok T, Park S. Nanotubular structured Si-based multi-component anodes for high-performance lithium-ion batteries with controllable pore size via coaxial electro-spinning. Nanoscale 2015;7:6126–35.
[9] Yu BC, Hwa Y, Park CM, Kim JH, Sohn HJ. Effect of oxide layer thickness to nano-Si anode for Li-ion batteries. Rsc Adv 2013;3:9408–13.
[10] Jeong S, Lee JP, Ko M, Kim G, Park S, Cho J. Etched graphite with Internally Grown Si nanowires from pores as an anode for high density Li-ion batteries. Nano Lett 2013;13:3403–7.
[11] Nguyen HT, Yao F, Zamfir MR, Biswas C, So KP, Lee YH, et al. Highly interconnected Si nanowires for improved stability Li-ion battery anodes. Adv Energy Mater 2011;1:1154–61.
[12] Sethuraman VA, Chon MJ, Shimshak M, Van Winkle N, Guduru PR. In situ measurement of biaxial modulus of Si anode for Li-ion batteries. Electrochem Commun 2010;12:1614–7.
[13] Li W, Zheng J, Chen TK, Wang T, Wang XJ, Li XG. One step preparation of a high performance Ge-C nanocomposite anode for lithium ion batteries by tandem plasma reactions. Chem Commun 2014;50:2052–4.
[14] Xu Y, Zhu XS, Zhou XS, Liu X, Liu YX, Dai ZH, et al. Ge nanoparticles encapsulated in nitrogen-doped reduced graphene oxide as an advanced anode material for lithium-ion batteries. J Phys Chem C 2014;118:28502–8.
[15] Song T, Jeon Y, Samal M, Han H, Park H, Ha J, et al. A Ge inverse opal with porous walls as an anode for lithium ion batteries. Energ Environ Sci 2012;5:9028–33.
[16] Zhang N, Zhao Q, Han XP, Yang JG, Chen J. Pitaya-like Sn@C nanocomposites as high-rate and long-life anode for lithium-ion batteries. Nanoscale 2014;6:2827–32.

[17] Kaspar J, Terzioglu C, Ionescu E, Graczyk-Zajac M, Hapis S, Kleebe HJ, et al. Stable SiOC/Sn nanocomposite anodes for lithium-ion batteries with outstanding cycling stability. Adv Funct Mater 2014;24:4097–104.
[18] Polat DB, Lu J, Abouimrane A, Keles O, Amine K. Nanocolumnar structured porous Cu–Sn thin film as anode material for lithium-ion batteries. Acs Appl Mater Inter 2014;6:10877–85.
[19] Meschini I, Nobili F, Mancini M, Marassi R, Tossici R, Savoini A, et al. High-performance Sn@carbon nanocomposite anode for lithium batteries. J Power Sources 2013;226:241–8.
[20] Zhuo K, Jeong MG, Chung CH. Highly porous dendritic Ni-Sn anodes for lithium-ion batteries. J Power Sources 2013;244:601–5.
[21] Yoo S, Lee JI, Shin M, Park S. Large-scale synthesis of interconnected Si/SiO_x nanowire anodes for rechargeable lithium-ion batteries. Chemsuschem 2013;6:1153–7.
[22] Wang W, Tian M, Wei YJ, Lee SH, Lee YC, Yang RG. Binder-free three-dimensional silicon/carbon nanowire networks for high performance lithium-ion battery anodes. Nano Energy 2013;2:943–50.
[23] Yue C, Yu YJ, Wu ZG, He X, Wang JY, Li JT, et al. Enhanced reversible lithium storage in germanium nano-island coated 3D hexagonal bottle-like Si nanorod arrays. Nanoscale 2014;6:1817–22.
[24] Komaba S, Yabuuchi N, Ozeki T, Han ZJ, Shimomura K, Yui H, et al. Comparative study of sodium polyacrylate and poly(vinylidene fluoride) as binders for high capacity Si-graphite composite negative electrodes in Li-ion batteries. J Phys Chem C 2012;116:1380–9.
[25] Bogart TD, Oka D, Lu XT, Gu M, Wang CM, Korgel BA. Lithium ion battery peformance of silicon nanowires with carbon skin. Acs Nano 2014;8:915–22.
[26] Liu NA, Hu LB, McDowell MT, Jackson A, Cui Y. Prelithiated silicon nanowires as an anode for lithium ion batteries. Acs Nano 2011;5:6487–93.
[27] Yersak TA, Son SB, Cho JS, Suh SS, Kim YU, Moon JT, et al. An all-solid-state Li-ion battery with a pre-lithiated Si-Ti-Ni Alloy anode. J Electrochem Soc 2013;160:A1497–501.
[28] Wang CS, Wu GT, Zhang XB, Qi ZF, Li WZ. Lithium insertion in carbon-silicon composite materials produced by mechanical milling. J Electrochem Soc 1998;145:2751–8.
[29] Li H, Huang XJ, Chen LQ, Wu ZG, Liang Y. A high capacity nano-Si composite anode material for lithium rechargeable batteries. Electrochem Solid St 1999;2:547–9.
[30] Yi R, Dai F, Gordin ML, Chen SR, Wang DH. Micro-sized Si-C composite with interconnected nanoscale building blocks as high-performance anodes for practical application in lithium-ion batteries. Adv Energy Mater 2013;3:295–300.
[31] Li XL, Gu M, Hu SY, Kennard R, Yan PF, Chen XL, et al. Mesoporous silicon sponge as an anti-pulverization structure for high-performance lithium-ion battery anodes. Nat Commun 2014;5:4105.
[32] Kim H, Han B, Choo J, Cho J. Three-dimensional porous silicon particles for use in high-performance lithium secondary batteries. Angew Chem Int Ed 2008;47:10151–4.
[33] Tian H, Tan X, Xin F, Wang C, Han W. Micro-sized nano-porous Si/C anodes for lithium ion batteries. Nano Energy 2015;11:490–9.
[34] Jiang ZY, Li CL, Hao SJ, Zhu K, Zhang P. An easy way for preparing high performance porous silicon powder by acid etching Al-Si alloy powder for lithium ion battery. Electrochim Acta 2014;115:393–8.
[35] Bang BM, Kim H, Song HK, Cho J, Park S. Scalable approach to multi-dimensional bulk Si anodes via metal-assisted chemical etching. Energ Environ Sci 2011;4:5013–9.
[36] Bang BM, Lee JI, Kim H, Cho J, Park S. High-performance macroporous bulk silicon anodes synthesized by template-free chemical etching. Adv Energy Mater 2012;2:878–83.
[37] Lee JI, Choi NS, Park S. Highly stable Si-based multicomponent anodes for practical use in lithium-ion batteries. Energ Environ Sci 2012;5:7878–82.
[38] Yi R, Zai JT, Dai F, Gordin ML, Wang DH. Dual conductive network-enabled graphene/Si-C composite anode with high areal capacity for lithium-ion batteries. Nano Energy 2014;6:211–8.
[39] Kim JS, Halim M, Byun D, Lee JK. Amorphous carbon-coated prickle-like silicon of micro and nano hybrid anode materials for lithium-ion batteries. Solid State Ionics 2014;260:36–42.
[40] Song JX, Chen SR, Zhou MJ, Xu T, Lv DP, Gordin ML, et al. Micro-sized silicon-carbon composites composed of carbon-coated sub-10 nm Si primary particles as high-performance anode materials for lithium-ion batteries. J Mater Chem A 2014;2:1257–62.
[41] Wang DS, Gao MX, Pan HG, Liu YF, Wang JH, Li SQ, et al. Enhanced cycle stability of micro-sized Si/C anode material with low carbon content fabricated via spray drying and in situ carbonization. J Alloy Compd 2014;604:130–6.
[42] He YS, Gao PF, Chen J, Yang XW, Liao XZ, Yang J, et al. A novel bath lily-like graphene sheet-wrapped nano-Si composite as a high performance anode material for Li-ion batteries. Rsc Adv 2011;1:958–60.
[43] Kierzek K, Machnikowski J, Beguin F. Towards the realistic silicon/carbon composite for Li-ion secondary battery anode. J Appl Electrochem 2015;45:1–10.
[44] Wang C, Wu H, Chen Z, McDowell MT, Cui Y, Bao ZA. Self-healing chemistry enables the stable operation of silicon microparticle anodes for high-energy lithium-ion batteries. Nat Chem 2013;5:1042–8.
[45] Rousselot S, Gauthier M, Mazouzi D, Lestriez B, Guyomard D, Roue L. Synthesis of boron-doped Si particles by ball milling and application in Li-ion batteries. J Power Sources 2012;202:262–8.
[46] Vankooten JJ, Weller GA, Ammerlaan CAJ. Electron-paramagnetic resonance on iron-acceptor pairs in silicon. Phys Rev B 1984;30:4564–70.
[47] Krishnan R, Lu TM, Koratkar N. Functionally strain-graded nanoscoops for high power Li-ion battery anodes. Nano Lett 2011;11:377–84.
[48] Ge MY, Rong JP, Fang X, Zhou CW. Porous doped silicon nanowires for lithium ion battery anode with long cycle life. Nano Lett 2012;12:2318–23.
[49] Liu B, Wang XF, Chen HT, Wang ZR, Chen D, Cheng YB, et al. Hierarchical silicon nanowires-carbon textiles matrix as a binder-free anode for high-performance advanced lithium-ion batteries. Sci Rep UK 2013;3.
[50] Xue LG, Fu K, Li Y, Xu GJ, Lu Y, Zhang S, et al. Si/C composite nanofibers with stable electric conductive network for use as durable lithium-ion battery anode. Nano Energy 2013;2:361–7.
[51] Xu YH, Zhu YJ, Han FD, Luo C, Wang CS. 3D Si/C fiber paper electrodes fabricated using a combined Electrospray/Electrospinning technique for Li-ion batteries. Adv Energy Mater 2015;5:1400753.
[52] Wang XL, Han WQ. Graphene enhances Li storage capacity of porous single-crystalline silicon nanowires. ACS Appl Mater Inter 2010;2:3709–13.
[53] Yuan FW, Yang HJ, Tuan HY. Alkanethiol-passivated Ge nanowires as high-performance anode materials for lithium-ion batteries: the role of chemical surface functionalization. Acs Nano 2012;6:9932–42.
[54] Liu J, Song KP, Zhu CB, Chen CC, van Aken PA, Maier J, et al. Ge/C nanowires as high-capacity and long-life anode materials for Li-ion batteries. ACS Nano 2014;8:7051–9.
[55] Ngo DT, Kalubarme RS, Le HTT, Fisher JG, Park CN, Kim ID, et al. Carbon-interconnected Ge nanocrystals as an anode with ultra-long-term cyclability for lithium ion batteries. Adv Funct Mater 2014;24:5291–8.
[56] Li D, Seng KH, Shi DQ, Chen ZX, Liu HK, Guo ZP. A unique sandwich-structured C/Ge/graphene nanocomposite as an anode material for high power lithium ion batteries. J Mater Chem A 2013;1:14115–21.
[57] Li XN, Liang JW, Hou ZG, Zhu YC, Wang Y, Qian YT. A synchronous approach for facile production of Ge-carbon hybrid nanoparticles for high-performance lithium batteries. Chem Commun 2015;51:3882–5.
[58] Fang S, Shen LF, Zheng H, Zhang XG. Ge–graphene–carbon nanotube composite anode for high performance lithium-ion batteries. J Mater Chem A 2015;3:1498–503.
[59] Lv DP, Gordin ML, Yi R, Xu T, Song JX, Jiang YB, et al. GeO_x/reduced graphene oxide composite as an anode for Li-ion batteries: enhanced capacity via reversible utilization of Li_2O along with improved rate performance. Adv Funct Mater 2014;24:1059–66.
[60] Chan CK, Zhang XF, Cui Y. High capacity Li ion battery anodes using Ge nanowires. Nano Lett 2008;8:307–9.
[61] Yan CL, Xi W, Si WP, Deng JW, Schmidt OG. Highly conductive and strain-released hybrid multilayer Ge/Ti nanomembranes with enhanced lithium-ion-storage capability. Adv Mater 2013;25:539–44.

[62] Seng KH, Park MH, Guo ZP, Liu HK, Cho J. Catalytic role of Ge in highly reversible GeO_2/Ge/C nanocomposite anode material for lithium batteries. Nano Lett 2013;13:1230–6.
[63] Wang JZ, Du N, Zhang H, Yu JX, Yang DR. Cu-Ge core-shell nanowire arrays as three-dimensional electrodes for high-rate capability lithium-ion batteries. J Mater Chem 2012;22:1511–5.
[64] Zhang CJ, Pang SP, Kong QS, Liu ZH, Hu H, Jiang W, et al. An elastic germanium-carbon nanotubes-copper foam monolith as an anode for rechargeable lithium batteries. Rsc Adv 2013;3:1336–40.
[65] Hwang CM, Park JW. Electrochemical characterization of a Ge-based composite film fabricated as an anode material using magnetron sputtering for lithium ion batteries. Thin Solid Films 2010;518:6590–7.
[66] Hwang CM, Lim CH, Park JW. Evaluation of Si/Ge multi-layered negative film electrodes using magnetron sputtering for rechargeable lithium ion batteries. Thin Solid Films 2011;519:2332–8.
[67] Jia HP, Kloepsch R, He X, Badillo JP, Gao PF, Fromm O, et al. Reversible storage of lithium in three-dimensional macroporous germanium. Chem Mater 2014;26:5683–8.
[68] Kim H, Son Y, Park C, Cho J, Choi HC. Catalyst-free direct growth of a single to a few layers of graphene on a germanium nanowire for the anode material of a lithium battery. Angew Chem Int Ed 2013;52:5997–6001.
[69] Wang XL, Han WQ, Chen HY, Bai JM, Tyson TA, Yu XQ, et al. Amorphous hierarchical porous GeOx as high-capacity anodes for Li ion batteries with very long cycling life. J Am Chem Soc 2011;133:20692–5.
[70] Liu M, Ma X, Gan L, Xu Z, Zhu D, Chen L. A facile synthesis of a novel mesoporous Ge@C sphere anode with stable and high capacity for lithium ion batteries. J Mater Chem A 2014;2:17107–14.
[71] Li X, Liang J, Hou Z, Zhu Y, Wang Y, Qian Y. A synchronous approach for facile production of Ge–carbon hybrid nanoparticles for high-performance lithium batteries. Chem Commun 2015;51:3882–5.
[72] Xue DJ, Xin S, Yan Y, Jiang KC, Yin YX, Guo YG, et al. Improving the electrode performance of Ge through Ge@C core-shell nanoparticles and graphene networks. J Am Chem Soc 2012;134:2512–5.
[73] Jahel A, Darwiche A, Ghimbeu CM, Vix-Guterl C, Monconduit L. High cycleability nano-GeO_2/mesoporous carbon composite as enhanced energy storage anode material in Li-ion batteries. J Power Sources 2014;269:755–9.
[74] Qiu H, Zeng L, Lan T, Ding X, Wei M. In situ synthesis of GeO_2/reduced graphene oxide composite on Ni foam substrate as a binder-free anode for high-capacity lithium-ion batteries. J Mater Chem A 2015;3:1619–23.
[75] Jin SX, Li N, Cui H, Wang CX. Embedded into graphene Ge nanoparticles highly dispersed on vertically aligned graphene with excellent electrochemical performance for lithium storage. ACS Appl Mater Interfaces 2014;6:19397–404.
[76] Ngo DT, Kalubarme RS, Le HTT, Park CN, Park CJ. Conducting additive-free amorphous GeO_2/C composite as a high capacity and long-term stability anode for lithium ion batteries. Nanoscale 2015;7:2552–60.
[77] Park MH, Kim K, Kim J, Cho J. Flexible dimensional control of high-capacity Li-ion-battery anodes: from 0D hollow to 3D porous germanium nanoparticle assemblies. Adv Mater 2010;22:415–8.
[78] Idota Yoshio, Kubota Tadahiko, Matsufuji Akihiro, Maekawa Yukio, Miyasaka T. Tin-based amorphous oxide: a high-capacity lithium-ion-storage material. Science 1997;276:1395–7.
[79] Wang Y-X, Lim Y-G, Park M-S, Chou S-L, Kim JH, Liu H-K, et al. Ultrafine SnO_2 nanoparticle loading onto reduced graphene oxide as anodes for sodium-ion batteries with superior rate and cycling performances. J Mater Chem A 2014;2:529–34.
[80] Oro S, Urita K, Moriguchi I. Enhanced charge-discharge properties of SnO_2 nanocrystallites in confined carbon nanospace. Chem Commun 2014;50:7143–6.
[81] Nobili F, Meschini I, Mancini M, Tossici R, Marassi R, Croce F. High-performance Sn@carbon nanocomposite anode for lithium-ion batteries: lithium storage processes characterization and low-temperature behavior. Electrochim Acta 2013;107:85–92.
[82] Liu H, Hu R, Sun W, Zeng M, Liu J, Yang L, et al. Sn@SnO_x/C nanocomposites prepared by oxygen plasma-assisted milling as cyclic durable anodes for lithium ion batteries. J Power Sources 2013;242:114–21.
[83] Gu Y, Wu F, Wang Y. Confined volume change in Sn-Co-C ternary tube-in-tube composites for high-capacity and long-life lithium storage. Adv Funct Mater 2013;23:893–9.
[84] Xu Y, Zhu Y, Liu Y, Wang C. Electrochemical performance of porous carbon/tin composite anodes for sodium-ion and lithium-ion batteries. Adv Energy Mater 2013;3:128–33.
[85] Tarascon J-M, A M. Issues and challenges facing rechargeable lithium batteries. Nature 2001;414:359–67.
[86] Liu YH, Xu YH, Zhu YJ, Culver JN, Lundgren CA, Xu K, et al. Tin-coated viral nanoforests as sodium-ion battery anodes. Acs Nano 2013;7:3627–34.
[87] Xu YH, Guo JC, Wang CS. Sponge-like porous carbon/tin composite anode materials for lithium ion batteries. J Mater Chem 2012;22:9562–7.
[88] Xu WW, Zhao KN, Niu CJ, Zhang L, Cai ZY, Han CH, et al. Heterogeneous branched core-shell SnO_2-PANI nanorod arrays with mechanical integrity and three dimensional electron transport for lithium batteries. Nano Energy 2014;8:196–204.
[89] Liu RQ, Li DY, Wang C, Li N, Li Q, Lu XJ, et al. Core-shell structured hollow SnO2-polypyrrole nanocomposite anodes with enhanced cyclic performance for lithium-ion batteries. Nano Energy 2014;6:73–81.
[90] Jeong M, Yokoshima T, Nara H, Momma T, Osaka T. Effect of electrolyte on cycle performances of the electrodeposited Sn-O-C composite anode of lithium secondary batteries. J Power Sources 2015;275:525–30.
[91] Kim HS, Yu SH, Cho YH, Kang SH, Sung YE. TiO2-core/Sn-shell nanotube arrays based on monolithic negative electrode for Li-ion batteries. Electrochim Acta 2014;130:600–5.
[92] Birrozzi A, Raccichini R, Nobili F, Marinaro M, Tossici R, Marassi R. High-stability graphene nano sheets/SnO_2 composite anode for lithium ion batteries. Electrochim Acta 2014;137:228–34.
[93] Bhaskar A, Deepa M, Rao TN. Size-controlled SnO_2 hollow spheres via a template free approach as anodes for lithium ion batteries. Nanoscale 2014;6:10762–71.
[94] Bhaskar A, Deepa M, Ramakrishna M, Rao TN. Poly(3,4-ethylenedioxythiophene) sheath over a SnO_2 hollow spheres/graphene oxide hybrid for a durable anode in Li-ion batteries. J Phys Chem C 2014;118:7296–306.
[95] Fan Q, Chupas PJ, Whittingham MS. Characterization of amorphous and crystalline tin–cobalt anodes. Electrochem Solid-State Lett 2007;10:A274–8.
[96] Wang X-L, Han W-Q, Chen J, Graetz J. Single-crystal intermetallic M–Sn (M = Fe, Cu, Co, Ni) nanospheres as negative electrodes for lithium-ion batteries. ACS Appl Mat Interfaces 2010;2:1548–51.
[97] Chou NH, Schaak RE. Shape-Controlled conversion of Beta-Sn nanocrystals into intermetallic M-Sn (M = Fe, Co, Ni, Pd) nanocrystals. J Am Chem Soc 2007;129:7339–45.
[98] Vasquez Y, Henkes AE, Chris Bauer J, Schaak RE. Nanocrystal conversion chemistry: a unified and materials-general strategy for the template-based synthesis of nanocrystalline solids. J Solid State Chem 2008;181:1509–23.
[99] Wang Xiao-Liang, F M, Aronson Meigan C, Han Wei-Qiang. $SnSnO_x$ core-shell nanospheres synthesis, anode performance in Li ion batteries, and superconductivity. J Phys Chem C 2010;114:14697–703.
[100] Wang X-L, Feygenson M, Chen H, Lin C-H, Ku W, Bai J, et al. Nanospheres of a new intermetallic $FeSn_5$ phase: synthesis, magnetic properties and anode performance in Li-ion batteries. J Am Chem Soc 2011;133:11213–9.
[101] Wang X-L, Chen H, Bai J, Han W-Q. $CoSn_5$ phase: crystal structure resolving and stable high capacity as anodes for Li ion batteries. J Phys Chem Lett 2012;3:1488–92.
[102] Xin F, Wang X, Bai J, Wen W, Tian H, Wang C, et al. A lithiation/delithiation mechanism of monodispersed MSn_5 (M = Fe, Co and FeCo) nanospheres. J Mater Chem A 2015;3:7170–8.
[103] Wolfenstine J, Campos S, Foster D, Read J, Behl WK. Nano-scale Cu_6Sn_5 anodes. J Power Sources 2002;109:230–3.

[104] Trahey L, Vaughey JT, Kung HH, Thackeray MM. High-capacity, microporous Cu_6Sn_5-Sn anodes for Li-ion batteries. J Electrochem Soc 2009;156:A385–9.
[105] Polat BD, Sezgin N, Kele Ö, Kazmanlı K, Abouimbrane A, Amine K. Cu-Sn thin film production on copper substrate. Electrochem Soc 2013;50:279–92.
[106] Mao O, Dahn JR. Mechanically alloyed Sn-Fe(-C) powders as anode materials for Li-ion batteries – III. Sn_2Fe: SnFe3C active/inactive composites. J Electrochem Soc 1999;146:423–7.
[107] Zhang CQ, Tu JP, Huang XH, Yuan YF, Wang SF, Mao F. Preparation and electrochemical performances of nanoscale $FeSn_2$ as anode material for lithium ion batteries. J Alloys Compd 2008;457:81–5.
[108] Nwokeke UG, Chadwick AV, Alcantara R, Alfredsson M, Tirado JL. Nanocrystalline $Fe_{1-x}Co_xSn_2$ solid solutions prepared by reduction of salts in tetraethylene glycol. J Alloys Compd 2011;509:3074–9.
[109] Dahn JR, Mar RE, Abouzeid A. Combinatorial study of $Sn_{1-x}Co_x$ ($0 < x < 0.6$) and $Sn_{0.55}Co_{0.45(1-y)}C_y$ ($0 < y < 0.5$) alloy negative electrode materials for Li-ion batteries. J Electrochem Soc 2006;153:A361–5.
[110] Hassoun J, Panero S, Mulas G, Scrosati B. An electrochemical investigation of a Sn-Co-C ternary alloy as a negative electrode in Li-ion batteries. J Power Sources 2007;171:928–31.
[111] Lee S-I, Yoon S, Park C-M, Lee J-M, Kim H, Im D, et al. Reaction mechanism and electrochemical characterization of a Sn-Co-C composite anode for Li-ion batteries. Electrochim Acta 2008;54:364–9.
[112] Kim Y-L, Lee H-Y, Jang S-W, Lee S-J, Baik H-K, Yoon Y-S, et al. Nanostructured Ni_3Sn_2 thin film as anodes for thin film rechargeable lithium batteries. Solid State Ionics 2003;160:235–40.
[113] Mukaibo H, Momma T, Osaka T. Changes of electro-deposited Sn-Ni alloy thin film for lithium ion battery anodes during charge discharge cycling. J Power Sources 2005;146:457–63.
[114] Liu J, Wen Y, van Aken PA, Maier J, Yu Y. Facile synthesis of highly porous Ni-Sn intermetallic microcages with excellent electrochemical performance for lithium and sodium storage. Nano Lett 2014;14:6387–92.
[115] Yu Y, Gu L, Wang C, Dhanabalan A, van Aken PA, Maier J. Encapsulation of Sn@Carbon nanoparticles in bamboo-like hollow carbon nanofibers as an anode material in lithium-based batteries. Angew Chem Int Ed 2009;48:6485–9.
[116] Wang Y, Wu M, Jiao Z, Lee JY. Sn@CNT and Sn@C@CNT nanostructures for superior reversible lithium ion storage. Chem Mater 2009;21:3210–5.
[117] Luo B, Wang B, Li X, Jia Y, Liang M, Zhi L. Graphene-confined Sn nanosheets with enhanced lithium storage capability. Adv Mater 2012;24:3538–43.
[118] Zheng XY, Lv W, He YB, Zhang C, Wei W, Tao Y, et al. 3D hollow Sn@Carbon-graphene hybrid material as promising anode for lithium-ion batteries. J Nanomater 2014;974285:1–6.
[119] Xu Y, Liu Q, Zhu Y, Liu Y, Langrock A, Zachariah MR, et al. Uniform nano-Sn/C composite anodes for lithium ion batteries. Nano Lett 2013;13:470–4.
[120] Zhu Z, Wang S, Du J, Jin Q, Zhang T, Cheng F, et al. Ultrasmall Sn nanoparticles embedded in nitrogen-doped porous carbon as high-performance anode for lithium-ion batteries. Nano Lett 2014;14:153–7.
[121] Qin J, He CN, Zhao NQ, Wang ZY, Shi CS, Liu EZ, et al. Graphene networks anchored with Sn@graphene as lithium ion battery anode. ACS Nano 2014;8:1728–38.
[122] Xin F, Tian H, Wang X-L, Xu W, Zheng W, Han W-Q. Enhanced electrochemical performance of $Fe_{0.74}Sn_5$@ reduced graphene oxide nanocomposite anode for both Li-ion and Na-ion batteries. ACS Appl Mat Interfaces 2015;7:7912–9.
[123] Xu L, Kim C, Shukla AK, Dong A, Mattox TM, Milliron DJ, et al. Monodisperse Sn nanocrystals as a platform for the study of mechanical damage during electrochemical reactions with Li. Nano Lett 2013;13:1800–5.
[124] Lee Y, Jo MR, Song K, Nam KM, Park JT, Kang Y-M. Hollow Sn-SnO_2 nanocrystal/graphite composites and their lithium storage properties. ACS Appl Mat Interfaces 2012;4:3459–64.

Huajun Tian is currently working as a research fellow in Ningbo Institute of Materials Technology and Engineering (NIMTE), Chinese Academy of Sciences. He received his B,S. degree in China University of Geosciences(Wuhan) and earned his Ph.D. degree in Materials Physics and Chemistry from Institute of Plasma Physics, Chinese Academy of Sciences in 2013. From 2012 to 2014, he conducted postdoctoral research in Professor Weiqiang Han's research group at NIMTE, Chinese Academy of Sciences. His research interests are energy storage devices, including Lithium-ion Batteries and Sodium ion Batteries.

Fengxia Xin is currently a PhD candidate at Ningbo Institute of Materials Technology and Engineering (NIMTE), Chinese Academy of Sciences. She obtained her BS degree in China Jiliang University in China in 2012. Her research interests are mainly on nanomaterials for energy storage in Li-ion and Na-ion batteries.

Xiao-Liang Wang is currently a R&D Manager at Seeo Inc. Before coming to Seeo, he was a research associate at Brookhaven National Laboratory (BNL). At BNL he was using nanostructuring as a tool to explore the synthesis of high-performance electrode nanomaterials for lithium batteries and to study fundamental mechanisms. He has 12 papers as the first author and more than 600 citations. He is an inventor on 4 US patent applications and 2 Chinese patents.

Wei He is currently a M.S. candidate under supervision of Prof. Wei-Qiang Han at Ningbo Institute of Materials Technology and Engineering (NIMTE), Chinese Academy of Sciences. He received his B.S. degree from Department of Materials Science and Engineering at Zhejiang University in 2013. His research mainly focuses on Si-based anode materials for energy storage devices in Li-ion batteries.

Wei-Qiang Han is currently a professor and the director of Institute of New Energy Technology at the Ningbo Institute of Materials Technology and Engineering (NIMTE), Chinese Academy of Sciences. He has published more than 100 paper in peer-reviewed journals. He has been developing novel nanomaterials for the applications of renewable energies, especially for advanced lithium batteries and catalysts.